1	Main Manuscript for
2 3	Hygroscopicity of Isoprene-Derived Secondary Organic Aerosol Mixture Proxies: Importance of Diffusion and Salting In Effects
4 5 6	Nahin Ferdousi-Rokib <sup>1*</sup> , N. Cazimir Armstrong <sup>2</sup> , Stephanie Jacoby <sup>3</sup> , Alana J. Dodero <sup>4</sup> , Martin Ahn <sup>1</sup> , Ergine R. Remy <sup>1</sup> , Zhenfa Zhang <sup>2</sup> , Avram Gold <sup>2</sup> , Joseph L. Woo <sup>5</sup> , Yue Zhang <sup>4</sup> , Jason D. Surratt <sup>2,6</sup> , Akua A. Asa-Awuku <sup>1,3</sup>
7 8	<sup>1</sup> Department of Chemical and Biomolecular Engineering, University of Maryland, College Park, MD 20742, United States
9 10	<sup>2</sup> Department of Environmental Sciences and Engineering, University of North Carolina at Chapel Hill, Chapel Hill, North Carolina 27599, United States
11 12	<sup>3</sup> Department of Chemistry and Biochemistry, University of Maryland, College Park, MD 20742, United States
13 14	<sup>4</sup> Department of Atmospheric Sciences, Texas A&M University, College Station, Texas 77843, United States
15 16	<sup>5</sup> Department of Chemical and Biomolecular Engineering, Lafayette College, Easton, PA 18042, United States
17 18	<sup>6</sup> Department of Chemistry, University of North Carolina at Chapel Hill, Chapel Hill, North Carolina 27599, United States
19 20	*Now at: Department of Environmental Health and Engineering, Whiting School of Engineering, Johns Hopkins University, Baltimore, MD 21218, United States
21	Keywords: Hygroscopicity, Organic Aerosols, IEPOX, SOA, viscosity, AFM
22 23	Correspondence to: Nahin Ferdousi-Rokib ( <u>ferdousn19@gmail.com</u> ) and Akua A. Asa-Awuku ( <u>asaawuku@umd.edu</u> )
24	
25	
26	
27	
28	
29	
30	
31 32 33	Author Contributions: NF designed, collected, analyzed all experimental data, and analyzed theoretical models. CA contributed to design and analysis of water uptake data. SJ contributed to design and collection of H TDMA experimental data. AD contributed to design and analysis of

AFM data. MA contributed to design and collection of AFM data. ERR contributed to collection of surface tension experimental data. ZZ and AG contributed to sample synthesis. JLW contributed to design, collection, and analysis of dynamic surface tension experimental data. YZ contributed to viscosity, diffusion, and AFM data analysis. All authors contributed to the writing and preparation of the manuscript.

Competing Interest Statement: The authors have no competing interests to declare

Abstract

Isoprene-derived secondary organic aerosol (SOA) constituents, such as the 2-methyltetrols (2-MT) and 2-methyltetrol sulfates (2-MTS), have been readily detected in atmospheric fine aerosols (PM<sub>2.5</sub>). Isoprene-derived SOA compounds exist) and within aerosol mixtures containing inorganie salts, such as ammonium sulfate (AS). Despite its prevalence within the atmosphere, the water uptake of 2-MT, 2-MTS, and their mixtures are not well understood. In this study, we determine the physicochemical properties (e.g., surface activity, diffusivity, phase morphology) of synthesized 2-MT, 2-MTS samples, and their mixtures with AS. 2-MT and 2-MTS have been previously identified as surface-active compounds and are both considered viscous; thus, Thus, dynamic surface tension ( $\sigma_{s/a}$ ) measurements were taken for both compounds to determine their organic diffusion coefficients ( $D_s$ ). The droplet growth of the synthesized organic compounds and AS mixtures was measured under subsaturated conditions (< 100% RH) using a humidified tandem differential mobility analyzer (H-TDMA) and relative humidity (RH) was kept constant at 88.2% RH ± 1.5%. AerosolDroplet activation and droplet growth was alsowas measured under supersaturated (> 100% RH) conditions using a cloud condensation nuclei counter (CCNC); supersaturation (SS) ranged from 0.3-1.4%. Both subsaturated and supersaturated hygroscopicity Hygroscopicity in both regimes were parameterized by the single hygroscopicity parameter κ. Furthermore, aerosol viscosity and phase morphology were analyzed using atomic force microscopy (AFM) measurements.

This study demonstrates how diffusion and salting-in effects influence the water uptake of synthesized, isoprene-derived SOA mixtures such as 2 MT/AS and 2 MTS/AS. Results show that when mixed with AS, organic diffusion for 2-MTS/AS becomes an order of magnitude greater than for the organic solute alone; faster while 2-MT diffusivity remains unchanged in the presence of AS. Both 2-MT/AS and 2-MTS aerosols present a plateau in sub- and supersaturated subsaturated κ-values close to pure AS; 2-MTS/AS aerosols exhibit a similar behavior under subsaturated conditions. However, under supersaturated conditions, 2-MTS/AS behaves as an idealideally, well-mixed aerosol, and can be characterized by traditional κ-Köhler theory. Isoprene-derived SOA like 2-MT and 2-MTS samples are ubiquitous, and thus, the impact from biogenic sources and its non-ideal thermodynamic properties must be considered in aerosol-cloud interactions.

Formatted: Font: Times New Roman, 12 pt

Formatted: Justified

Formatted: Left

#### 1. Introduction

 Fine aerosol particles (PM2.5) suspended within our atmosphere are a major contributor to Earth's radiative forcing and uncertainties in global temperature projections (Intergovernmental Panel on Climate, 2023). Aerosol-cloud radiative forcing uncertainty is attributed to aerosols' ability to form and modify cloud properties, known as aerosol-cloud interactions or the "aerosol indirect effect" (Köhler, 1936; Twomey, 1959; Twomey, 1974; Albrecht, 1989; Intergovernmental Panel on Climate, 2023). An aerosol's ability to alter droplet formation is dependent on its hygroscopicity or water uptake behavior under supersaturated conditions (RH > 100%). In the presence of water vapor, aerosols present a surface for condensation; droplet activation depends on aerosol particle chemical composition and size (Seinfeld & Pandis, 1998; Petters & Kreidenweis, 2007). The aerosol droplets can reach a point of unstable and uncontrollable growth, thereby acting as cloud condensation nuclei (CCN) (Köhler, 1936; Seinfeld & Pandis, 1998).

Droplet models can apply Köhler theory to estimate aerosol droplet growth and CCN activity (Köhler, 1936). In traditional Köhler theory, it is assumed that all aerosol solutes instantaneously dissolve and contribute to water uptake (Petters & Kreidenweis, 2007). Aerosol hygroscopicity is thus parameterized by Köhler theory through the single hygroscopicity parameter  $\kappa$ ;  $\kappa$  of mixed composition is often estimated by the Zdanovskii-Stokes-Robinson (ZSR) mixing rule and it is assumed that an individual solute's contribution to hygroscopicity is scaled by its volume fraction (Petters & Kreidenweis, 2007). Thus, knowing aerosol composition is critical for understanding CCN formation. However,  $\kappa$ -Köhler predictions of aerosol CCN activity neglect solute physicochemical properties that may alter droplet growth. Previous studies have shown that droplet-altering properties may be present within aerosols, such as the presence of complex

108 morphologies (e.g., inner core-outer layer), surface-activity, or salting in/salting out effects; as a 109 result, discrepancies between experimentally-determined  $\kappa$  and  $\kappa$ -Köhler predictions may occur 110

(Asa-Awuku & Nenes, 2007; Bertram et al., 2011; Song et al., 2013; Prisle & Mølgaard, 2018;

111 Riemer et al., 2019; Ott et al., 2020; Malek et al., 2023).

Field studies have observed the presence of internally mixed aerosols containing both inorganic 112 and organic compounds (Saxena, 1995; Murphy et al., 1998; Pratt & Prather, 2010). Inorganic 113 aerosols, primarily composed of salts like ammonium sulfate (AS) and sodium chloride have well-114 115 defined hygroscopic properties. The ionic behavior of inorganic compounds promotes instantaneous dissolution in water and contributes to CCN activation (Cziczo et al., 1997; Seinfeld, 116 2003; Rose et al., 2008; Laskina et al., 2015). However, fine organic aerosols (OA) pose a greater 117 challenge to aerosol hygroscopicity predictions. OA constitute 20-50% of atmospheric fine aerosol 118 mass and are diverse in composition. OA can be directly emitted into the atmosphere, referred to 119 as primary organic aerosols (POA) (Kanakidou et al., 2005). POA can originate from 120 anthropogenic (e.g., biomass burning and coal combustion) and biogenic (e.g., pollen) sources 121 (Seinfeld & Pandis, 1998; Kanakidou et al., 2005). In addition to POA, secondary organic aerosol 122 (SOA) can be formed through multigeneration gas-phase oxidation reactions of volatile organic 123 compounds (VOCs) or multiphase reactions of semi-/low-volatility organic compounds 124 (SVOCs/LVOCs) (Kanakidou et al., 2005). SOA is ubiquitous in the atmosphere, forming a major 125 component of fine OA mass (Zhang et al., 2007; Srivastava et al., 2022). For example, a study by 126 Zhang et al. (2007) found that SOA contributed 65% to 95% of OA mass in urban and remote 127 regions. Furthermore, SOA have been readily detected in mixtures with inorganic components, 128 such as AS (Yang et al., 2009; Zhu et al., 2017); indeed, a study by Zhu et al. (2017) estimated 129 66% of SOA as being internally mixed with sulfate. Thus, in addition to understanding pure 130 131 organic compounds, it is important to also study organic-inorganic interactions.

Previous studies have determined that a significant contributor to SOA is the aqueous-phase 132 chemical processing of isoprene-derived oxidation products (Claeys et al., 2004; Kanakidou et al., 133 134 2005). Isoprene is a VOC emitted from biogenic sources and is considered one of the most abundant biogenic VOCs (BVOCs). Isoprene emissions have been estimated to be ~ 500 Tg C 135 year<sup>-1</sup>, rivaling methane emissions (Guenther et al., 2012; Sindelarova et al., 2014). Under alkyl 136 peroxy radical (RO2\*) + hydroperoxy radical (HO2\*) dominant conditions, isoprene is 137 photochemically oxidized by gas-phase hydroxyl radicals (OH) to form large quantities of 138 isoprene-derived epoxydiols (IEPOX) (Paulot et al., 2009). IEPOX is then able to partition into 139 acidic sulfate-containing aerosol particles to produce isoprene-derived SOA (Surratt et al., 2010; 140 Lin et al., 2012; Gaston et al., 2014; Riva et al., 2019), which consists largely of 2-methyltetrols 141 (2-MT) and 2-methyltetrol sulfates (2-MTS). 142

Both 2-MT and 2-MTS were previously detected in atmospheric PM<sub>2.5</sub>. For example, a study by 143 Claeys et al. (2004) found that 2-MT contributed 2% of organic carbon detected in PM<sub>2.5</sub> collected 144 145 from the Amazon rainforest. Additional field studies have also found that 2-MTS can contribute 0.3-16.5% of total organic carbon in both the Amazon rainforest and Southeast US (Chan et al., 146 147 2010; Froyd et al., 2010; Hettiyadura et al., 2019; Riva et al., 2019; Chen et al., 2021; Hughes et 148 al., 2021). The formation of both compounds can also alter aerosol particle composition and phase 149 state (Zhang et al., 2019a; Zhang et al., 2019b). For example, 2-MT and 2-MTS have been observed to be in a semisolid or glassy state in aerosol particles (Chen et al., 2023). Highly viscous 150 SOA can exist in a glassy state; SOA viscosities can range from 10<sup>2</sup> to 10<sup>12</sup> Pa·s for ultraviscous 151 liquids or >10<sup>12</sup> Pa·s for amorphous, extremely viscous compounds (Virtanen et al., 2010; 152 Renbaum-Wolff et al., 2013; Zhang et al., 2015). Viscosity can influence organic solute dissolution 153 in droplets by slowing diffusion through the aqueous phase (Renbaum-Wolff et al., 2013). As a 154 result, slower organic diffusion rates can influence gas partitioning, particle shape, chemical aging, 155 156 multiphase reactions, and aerosol droplet growth (Riipinen et al., 2011; Shiraiwa & Seinfeld, 2012; 157 Zhang et al., 2015). Furthermore, studies incorporating SOA viscosity and phase state into larger, global-scale models have observed changes to CCN and ice nuclei (IN) formation predictions 158 (Riipinen et al., 2011; Shiraiwa et al., 2017; Wolf et al., 2021). Thus, probing the viscosity and 159 resulting diffusion limitations may be necessary for understanding 2-MT and 2-MTS water uptake 160 properties (Chen et al., 2023). 161

162

163

164

165

166

167

168 169

170 171

172 173

174

175 176

177

178

179

180

181

182

183

184

185

186

187

188 189

190

Similar to other complex organic mixtures, the water uptake ability of isoprene-derived SOA can be further complicated when mixed with inorganic components, such as AS. Previous studies have observed the presence of internally-mixed SOA/AS aerosols in both the southeast US and Amazon; in both regions a strong presence of 2-MT and 2-MTS has been observed (Chan et al., 2010; Froyd et al., 2010; Bondy et al., 2018; Riva et al., 2019; Wu et al., 2019). The presence of inorganic salts in aerosol mixtures can influence phase state based on organic physicochemical properties (Topping, 2010; Ruehl et al., 2012; Ruehl et al., 2016; Malek et al., 2023). Inorganic compounds can result in water solubility-limited and/or surface-active organics partitioning to a separated phase (Ruehl et al., 2012; Ruehl et al., 2016; Freedman, 2017; Kang et al., 2020). As a result, the partitioned aerosols can exhibit a phase separated morphology (e.g., but not limited to Ruehl et al., 2012; Ruehl et al., 2016; Freedman, 2017; Kang et al., 2020; Malek et al., 2023). However, inorganic salts may also enhance organic dissolution, known as "salting in" (Riva et al., 2019). For instance, studies have observed increased diffusion in viscous SOA particles through the aqueous droplet phase in the presence of inorganic salts (Reid et al., 2018; Jeong et al., 2022; Sheldon et al., 2023). Increased diffusion is a result of salts disrupting the hydrogen bonding network between neighboring organic molecules (Reid et al., 2018; Jeong et al., 2022; Sheldon et al., 2023). Therefore, organic physicochemical properties (surface-activity, viscosity) of SOA, such as 2-MT and 2-MTS, must be better defined to better predict mixed SOA/AS aerosol CCN activity. To our knowledge there are no studies to date that investigate 2-MT and 2-MTS aerosol water uptake, water uptake of mixtures with AS, and the potential effect of physicochemical properties on CCN activity predictions.

In this study, we investigated the surface activity, diffusivity, droplet growth and water uptake of 2-MT, 2-MTS, and their mixtures with AS. 2-MT and 2-MTS surface tension values were experimentally determined. A previous study by Ekström et al. (2009) found 2-MT to be moderately surface-active. However, the surface activity of 2-MTS has not been characterized and potential organic surface tension depression in the presence of AS has not been explored for both organics. In tandem with surface tension measurements, this study estimated diffusion coefficients of both compounds to explore the effects of viscosity and diffusivity on aerosol water uptake. Aerosol κ-hygroscopicity for pure organic and organic-AS mixtures were experimentally

determined under both subsaturated conditions (< 100% RH) and supersaturated (> 100% RH) conditions to observe both droplet growth and CCN activity, respectively.  $\kappa$ -hygroscopicity measurements were then compared to  $\kappa$ -Köhler hygroscopicity theory to evaluate the efficacy of traditional full dissolution and negligible viscosity assumptions in predicting the CCN activity of both compounds and their mixtures. Lastly, Atomic Force Microscopy (AFM) measurements on mixed particles were conducted to further understand particle morphology. The following work provides a comprehensive analysis of the wide range of physicochemical properties that may influence the droplet growth of 2-MT and 2-MTS mixed with AS.

#### 2. Experimental Methods

#### 2.1. Experimental Chemicals

For this study, ammonium sulfate (AS, (NH<sub>4</sub>)<sub>2</sub>SO<sub>4</sub>; Thermo Fisher Scientific, >99.0%), was purchased and used without further purification. 2-methyltetrol (2-MT) and 2-methyltetrol sulfate (2-MTS) samples were synthesized using the published procedure of Cui et al. (2018). 2-MT was determined to be > 98% pure. The purity of 2-MTS was determined to be ~73 wt%, with remaining sample mass estimated to be 3 wt% AS and 24 wt% sodium methyl sulfate (SMS). It should be noted that from hereon 2-MTS sample refers to prescribed synthesized mixture and subsequent calculations account for the estimated contributions of AS and SMS.

#### 2.2. Surface Tension Measurements

The surface tension of 2-MT, 2-MTS, and their mixtures with AS was measured at atmospherically relevant aqueous phase concentrations. Due to the limited amounts of synthesized sample, mixed amounts were judiciously selected to mimic mixture ratios previously reported in the literature. Specifically, a study by Cope et al. (2021) found that 2-MT concentrations in the atmosphere reached an upper bound of 300 mM. Therefore, stock solutions of 300 mM 2-MT and 2-MTS were prepared using deionized (DI) water. Furthermore, it is assumed that surface tension measurements at dilutions higher than 300 mM are also relevant for droplet growth. A study Bain et al. (2023) found that aerosol surface tension can be approximated from surface tension measurements of bulk mixtures composed of < 100 mM organic component. Additionally, recent studies (Mikhailov et al., 2024; Ferdousi-Rokib et al., 2025) also support the application of more dilute concentration regimes to predict droplet growth. A recent study by Mikhailov et al. (2024) found that surface tension depression observed in bulk dilute surface tension measurements was reflective of aerosol properties. Ferdousi-Rokib et al. (2025) also found that salting out effects can be approximated in mixtures having < 100 mM organic component. Thus, in this work, the stock solutions were diluted to a 3-94 mM range; each stock solution and subsequent dilution concentrations are provided in Supplemental Tables S1-S5. 

Droplet surface tension ( $\sigma_{s/a}$ ) was measured using a pendant drop tensiometer with a modified profile analysis tensiometer (SINTERFACE Inc.); the experimental set up has been described in Fertil et al. (2025). Briefly, the pendant drop tensiometer generates a droplet of solution (< 10  $\mu$ L) suspended from a 0.9-mm diameter needle (Beier et al., 2019; Fertil et al., 2025). Droplets remain

suspended for 300 s to reach equilibrium; at each time step ( $\sim 1$  s), the droplet  $\sigma_{s/a}$  was obtained from fitting the droplet curvature to the Young-Laplace Equation (Fordham & Freeth, 1948; Spelt, 1996; Padró et al., 2010). Surface tension measurements were run in triplicate; prior to each measurement, the tensiometer was flushed with DI water and  $\sim 2$  mL of solution. Measurements were obtained at ambient room conditions, with temperature range of 20.2-22 °C and relative humidity range of 40-45 % RH.

As the droplet equilibrates, surface tension changes, which is attributed to the accumulation of solute diffusing to the droplet surface (Joos & Rillaerts, 1981; Eastoe et al., 1998; Chernyshev & Skliar, 2015). As the solute saturates the surface, surface tension reaches equilibrium (Ross, 1945). The accumulation of solute at the surface and resulting concentration gradient within the droplet can be described by Fick's Second Law:

$$\frac{\partial c}{\partial t} = D_{\rm S} \frac{\partial^2 c}{\partial x^2},\tag{1}$$

242 where concentration over time  $\frac{\partial c}{\partial t}$  is proportional to the second derivative concentration over 243 position  $\frac{\partial^2 c}{\partial x^2}$  and the diffusion coefficient  $D_s$  (m<sup>2</sup> s<sup>-1</sup>). The dynamic surface tension can be correlated 244 with solute diffusion over time as (Joos & Rillaerts, 1981):

$$\sigma_t = \sigma_0 - 2RTC \left(\frac{D_s t}{\pi}\right)^{0.5},\tag{2}$$

where  $\sigma_0$  is the starting surface tension,  $\sigma_t$  is the surface tension at specified time t, R is the universal gas constant, T is temperature, and C is organic molar concentration. Here, evaporation effects are negligible during the short suspension times. Therefore, the organic molar concentration C is equivalent to the droplet solution concentration as Eq. 2 can then be rearranged to solve for  $D_s$  using dynamic surface tension measurements.

## 2.3. Aerosol Experimental Methods

#### 253 2.3.1. Aerosol Generation

Solutions of 0.1 g L<sup>-1</sup> total solute (2-MT, 2-MTS, and mixtures with AS) were prepared using ultra-purified Millipore water (18 M $\Omega$ ·cm). Mixtures compositions are provided in Table S6. Polydisperse aerosols were then generated by passing each aqueous solution through a constant output Collison Nebulizer (Atomizer, TSI 3076); the generated aerosols were then dried to < 5% RH using two silica gel dyers in series. Aerosols were then analyzed for their water uptake properties under sub- and supersaturated conditions. To determine aerosol phase morphology, atomic force microscopy (AFM) images were also obtained. In addition to water uptake and AFM measurements, organic density and shape factor were measured; for details on density and shape factor measurements, see Armstrong et al. (2025).

#### 2.3.2 Water Uptake Measurements

A humidified tandem differential mobility analyzer (H-TDMA) measured droplet growth under subsaturated conditions. Dry, polydisperse aerosols were size selected at 100, 150, and 200 nm by an electrostatic classifier (DMA 1, TSI 3082; flow rate = 0.3 L min<sup>-1</sup>) and humidified using a Nafion humidification line (PermaPure M.H. series); particles were humidified at 88.2% ± 1.5% RH. Selected dry diameters are often assumed to be spherical, thus having a shape factor  $(\gamma)$  of 1 (DeCarlo et al., 2004). Aerodynamic aerosol classifier (AAC) shape factor measurements confirmed 2-MT and 2-MTS sphericity (Armstrong et al., 2025). The wet diameter (Dw) was measured using a second electrostatic classifier (DMA 2, TSI 3082; flow rate = 0.3 L min<sup>-1</sup>); the ratio of  $D_{\rm w}$  to the dry-size selected diameter ( $D_{\rm d}$ ) is equal to the growth factor ( $G_{\rm F}$ ). The experimental set up is provided in Fig. S1. To calibrate the H-TDMA, a 0.1 g L<sup>-1</sup> solution of AS was aerosolized; dried AS aerosols were size selected at 100 and 150 nm. Dried AS aerosol GF and instrument RH was measured, with calibration measurements repeated multiple times as reported in Table S7. The experimental solutions were then aerosolized, and  $G_F$  was obtained for each solution; GF is used to calculate the hygroscopicity parameter under subsaturated conditions,  $\kappa_{\text{H-TDMA}}$ . In addition to subsaturated conditions, water uptake was measured under supersaturated (SS) conditions using a CCNC-100 (Droplet Measurement Technologies); the experimental set up is provided in Fig. S2. The theory and operation of the CCNC has been previously described (Roberts & Nenes, 2005; Lance et al., 2006; Rose et al., 2008). The Scanning Mobility CCN Analysis (SMCA) protocol was used to measure droplet activation (Moore et al., 2010). Briefly, the dried polydisperse aerosols were passed through an electrostatic classifier (TSI 3080) in scanning mode and charged; scanning mode operated from 8-352 nm for 135 s. The DMA operated at a sheath-to-aerosol flow rate ratio of 10:1, and aerosol sample flow rate of 0.8 L min<sup>-1</sup>. The monodisperse, size-selected aerosol stream was then sampled by a condensation particle counter (CPC, TSI 3776, flow rate =  $0.3 L \text{ min}^{-1}$ ) and the CCNC-100 (flow rate =  $0.5 L \text{ min}^{-1}$ ) in parallel. The CPC counted the number concentration of dry particles at a given particle size (condensation nuclei,  $N_{CN}$ ). The CCNC exposed the particles to 0.3-1.4%SS and the number concentration of particles activated  $(N_{CCN})$  were measured. The instrument set up was calibrated using AS (Rose et al., 2008) and the calibration data are provided in Table S8 and Fig. S3.

The CPC counted the number concentration of dry particles at a given particle size (condensation nuclei,  $N_{CN}$ ). The CCNC exposed the particles to 0.3-1.4%SS and the number concentration of particles activated ( $N_{CCN}$ ) were measured. The instrument set up was calibrated using AS (Rose et al., 2008) and the calibration data are provided in Table S8 and Fig. S3.

296 CCN data of AS and experimental solutions were analyzed using the Python-based CCN Analysis 297 Toolkit (PyCAT 1.0) (Gohil, 2022; Gohil & Asa-Awuku, 2022). PyCAT is a Python version of SMCA and is available on GitHub for public use. The analysis toolkit calculated the activation 298 ratio  $N_{CCN}/N_{CN}$  for each dry particle size. The activation ratios were fitted using a sigmoid curve 299 and the critical diameter  $(D_{p,50})$  was found, at which ~50% of the dry particles activate. A charge 300 correction is applied in PyCAT using the multi-charge correction algorithm previously described 301 302 (Fuchs, 1963; Wiedensohler, 1988). The obtained critical diameter of each solution is then used to 303 calculate the single hygroscopicity parameter under supersaturated conditions,  $\kappa_{\rm CCN}$ .

304 2.3.3. Atomic Force Microscopy (AFM) Morphology

264

265

266

267

268

269

270 271

272

273

274

275

276

277278

279

280

281

282

283

284 285

286

287

288

289

290

Atomic force microscopy (AFM) measurements were utilized to characterize aerosol phase morphology. 2-MTS, 2-MTS/AS, and 2-MT/AS particles were collected onto silicon substrates (Silson Ltd) using a cascade impactor (Sioutas Cascade Impactor, flow rate = 9 L min<sup>-1</sup> and stored at room temperature and relative humidity (40-50% RH) prior to analysis. Imaging followed the procedure of Zhang et al. (2018). Briefly, particles were imaged in a 5 x 5  $\mu$ m region using a Dimension ICON® AFM (Bruker) in tapping mode with resonant frequency of 150 kHz and spring constant of 5.4 N m<sup>-1</sup>.

## 312 2.3.4 Viscosity and Diffusion Calculation

The viscosity and the diffusion coefficients of the 2-MT and 2-MTS aerosols were calculated using a modified Vogel-Tammann-Fulcher (VTF) equation (DeRieux et al., 2018). The dry glass transition temperature values were determined to be 226 K and 276 K from a previous study by Zhang et al. (2019b). The Gordon-Taylor coefficient and the fragility coefficient were assigned as 2.5 and 20, respectively. The hygroscopicity values were used from the measurement of H-TDMA of this study.

#### 3. Traditional κ-Köhler theory

Traditionally, water uptake of aerosol particles has been calculated using  $\kappa$ -Köhler theory (Köhler, 1936; Petters & Kreidenweis, 2007). Köhler theory considers aerosol physicochemical properties (e.g., solute density, molecular weight) to describe the equilibrium water vapor saturation ratio at a droplet's surface ( $S_{eq}$ ). The equilibrium relationship encompasses two competing effects. The Kelvin effect describes the increase of water vapor saturation as a result of the curvature of the droplet; the Kelvin effect is represented by droplet surface tension  $\sigma_{s/a}$ . The Raoult (solute) effect competes by decreasing vapor pressure due to the presence of solute in the aqueous droplet; the solute effect is represented by the water activity term,  $a_w$  (Seinfeld & Pandis, 1998; Wex et al., 2008). For compounds dissolved in water, water activity can be parameterized by the single hygroscopicity parameter,  $\kappa$ , as follows (Petters & Kreidenweis, 2007; Sullivan et al., 2009):

$$\frac{1}{a_{w}} = 1 + \kappa \frac{V_{s}}{V_{w}},\tag{3}$$

where  $V_{\rm w}$  and  $V_{\rm s}$  are the volume of water and dry solute, respectively. Therefore, the equilibrium saturation ratio ( $S_{\rm eq}$ ) over the droplet is described as:

$$S_{eq} = \left(1 + \kappa \frac{D_d^3}{D_w^3 - D_d^3}\right)^{-1} exp\left(\frac{4\sigma_{s/a}M_w}{RT\rho_w D_w}\right), \tag{4}$$

where  $\rho_{\rm w}$  is the density of water,  $M_{\rm w}$  is the molecular weight of water, R is the universal gas constant and T is the temperature.

 $\kappa$  describes ability of an aerosol to uptake water assuming full dissolution, and can be calculated 338 from the intrinsic properties of the solute as  $\kappa_{\text{int}}$  (Sullivan et al., 2009):

$$\kappa_{\rm int} = \frac{\nu_{\rm s}\rho_{\rm s}M_{\rm w}}{\rho_{\rm w}M_{\rm s}},\tag{5}$$

where  $M_s$  is the molecular weight of solute,  $v_s$  is the van't Hoff factor, and  $\rho_s$  is the density of the solute; Armstrong et al. (2025) found 2-MT and 2-MTS density to be 1.4 g cm<sup>-3</sup> and 2.46 g cm<sup>-3</sup>, respectively. To estimate  $\kappa$ -hygroscopicity of aerosols containing more than one compound, the Zdanovskii, Stokes, and Robinson (ZSR) mixing rule can be applied to estimate (Petters & Kreidenweis, 2007):

$$\kappa_{\rm ZSR} = \sum_{i} \varepsilon_i \kappa_i, \tag{6}$$

where  $\varepsilon_i$  is the volume fraction of the individual solute component, *i*.

Experimental data can be used to derive aerosol  $\kappa$ . Under subsaturated (< 100% RH) conditions,

348  $G_F$  is related to hygroscopicity as follows (Kreidenweis & Asa-Awuku, 2014):

349 
$$\kappa_{\text{H-TDMA}} = \frac{(G_F^{3-1})}{\frac{RH}{exp(\frac{4\sigma_{\text{S/a}}M_{\text{W}}}{RT\rho_{\text{W}}D_{\text{d}}G_F})}} - G_F^3 + 1, \tag{7}$$

Where  $\kappa_{\text{H-TDMA}}$  is subsaturated hygroscopicity and RH is the relative humidity of the H-TDMA instrument as a decimal. Similarly, for supersaturated (>100% RH), the critical diameter correlates to  $\kappa$  as follows (Petters & Kreidenweis, 2007):

353 
$$\kappa_{\text{CCN}} = \frac{4\left(\frac{4\sigma_{\text{S/a}}M_{\text{W}}}{RT\rho_{\text{W}}}\right)^{3}}{27D_{\text{S}}^{3} s_{\text{0}} ln^{2} SS}.$$
 (8)

Where  $\kappa_{\text{CCN}}$  is supersaturated hygroscopicity. It is assumed that droplet surface tension  $\sigma_{\text{S/a}}$  is equivalent to that of the surface tension of water  $\sim 72$  mN m<sup>-1</sup>. Köhler theory also assumes that all solutes are well mixed within the aqueous phase. The Köhler/ZSR model does not account for potential viscosity and diffusivity limitations due to inorganic-organic mixing in the aqueous phase. Therefore, in this study,  $\kappa$ - Köhler values are predicted assuming both 2-MT and 2-MTS are well mixed within the aqueous phase and fully contribute to droplet growth. The applicability of these assumptions is discussed in the later sections. Additionally, a list of variable abbreviations is provided in Table S9.

### 363 **4. Results**

354

355 356

357

358

359 360

361

- 364 4.1. Surface Tension and Diffusion
- 365 Organic Samples
- 366 Dynamic pendant drop tensiometer measurements were taken for 2-MT and 2-MTS samples;
- measurements were performed by hanging droplets  $\leq 10~\mu L$  over a period of 300 s. The droplet
- 368 curvature was measured every 1 s. Average surface tension values were obtained for 2-MT and 2-
- 369 MTS when droplet surface tension values remained constant (at equilibrium) and are listed in
- Table S10 and shown in Fig. 1.
- 371 In the dilute bulk measurement regime, 2-MT sample (Fig. 1, orange squares) and 2-MTS sample
- (Fig. 1, purple closed circles)  $\sigma_{s/a}$  values are close to pure water (~ 72 mN m<sup>-1</sup>, Fig. 1, blue dashed

line). For solutions < 53 mM organic concentration, 2-MT and 2-MTS samples exhibit little to no surface-activity. Surface-activity is similar to the dilute surface tension of pure AS, a non-surface-active compound, which remains ~ 72 mN m<sup>-1</sup>(Fig. 1, red circles, Pruppacher et al., 1997). However, for organic solutions > 53 mM, minimal surface tension depression is observed with  $\sigma_{s/a}$  values between ~68–70 mN m<sup>-1</sup> (Fig. 1 and Table S10); in comparison, AS surface tension increases with concentration, as observed in Fig. 1 and with previous studies (namely, Pruppacher et al., 1997; Hyvärinen et al., 2005; Mikhailov et al., 2024). Therefore, both synthesized 2-MT and 2-MTS sample mixtures can be classified as weakly surface-active. A previous study by Riva et al. (2019) observed greater surface tension depression for IEPOX SOA/sulfate mixtures. In particular, enhanced surface tension depression was attributed to organic partitioning and formation of 2-MT and 2-MTS oligomers (Riva et al., 2019).

 In comparison to the surface tension of other short-chained particulate organosulfates, such as sodium ethyl sulfate (Fig. 1, black triangles) and sodium methyl sulfate (Fig. 1, grey triangles), 2-MT and 2-MTS have lower dilute surface values (Peng et al., 2021). However, similar to other surface-active organosulfates (sodium ethyl sulfate and sodium octyl sulfate), neither 2-MT sample and 2-MTS sample surface tension significantly depress aerosol surface tension (Table S11 and S14). For example, Mikhailov et al. (2024) observed surface tension depression as low as ~ 56 mN m<sup>-1</sup> for dilute D-glucose/AS mixtures. Furthermore, moderately surface-active compounds, such as 2-methylglutaric acid (2-MGA, Fig. 1, green squares) and sodium octyl sulfate (Fig. 1, grey diamonds) exhibit surface tension depression in the range of ~ 64-68 mN m<sup>-1</sup> for concentrations  $\leq$  22 mM (Tables S13-S14). Additionally, stronger surface-active organics (surfactants), such as sodium dodecyl sulfate (SDS) show surface tension at the droplet surface can be depressed in the dilute regime. SDS reaches  $\sigma_{s/a}$  of ~ 39 mN m<sup>-1</sup> at 9 mM organic (Fig. 1 and Table S15). Sodium octyl sulfate, SDS, and 2-MGA present noticeable surface tension depression in the dilute bulk measurement regime (Fig. 1) that affect aerosol properties (Vepsäläinen et al., 2023; Zhang et al., 2023; Kleinheins et al., 2025). However, in comparison to

previously studied organics, 2-MT and 2-MTS  $\sigma_{s/a}$  samples remain close to pure water in the dilute bulk regime (Fig. 1). Previous studies by Bain et al. (2023) and Werner et al. (2025) emphasize the role of surface area-to-volume ratio dictating aerosol surface tension. Specifically, aerosol surface tension values are best represented by surface tension measurements of the organic in bulk solutions < 100 mM (Bain et al., 2023; Ferdousi-Rokib et al., 2025; Werner et al., 2025). Thus, 2-MT and 2-MTS sample mixture surface activity is negligible for droplet activation as both dilute organic  $\sigma_{s/a}$  is close to that of pure water (~72 mN m<sup>-1</sup>).

It should be <u>reiterated and</u> noted that the synthesized 2-MTS sample is 73% pure 2-MTS and is likely mixed with AS and SMS. Both SMS and AS (Fig.1, red circles; Table S16) have surface

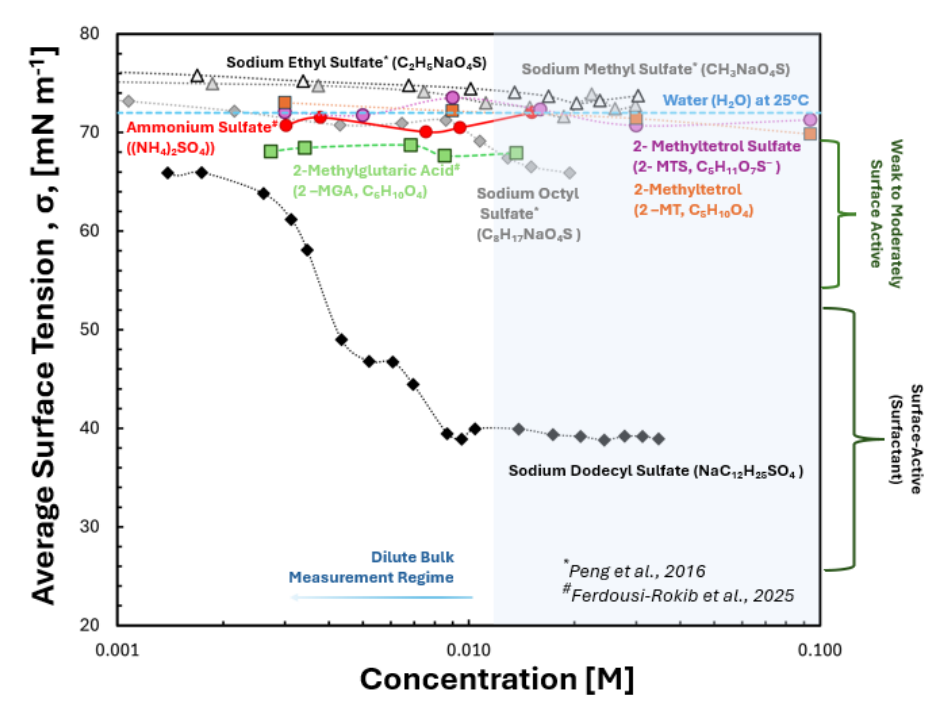


Figure 1. Experimental average surface tension  $\sigma_{\omega_0}$  values of compounds as a function of concentration. Average equilibrium surface tension of synthesized 2 MT and 2 MTS are shown as closed orange squares and closed purple circles, respectively. The surface tension of the organosulfates, including sodium ethyl sulfate (black open triangles), sodium methyl sulfate (grey closed triangles), and sodium octyl sulfate (grey closed diamonds) were obtained by Peng et al. (2016). 2 methylglutaric acid (green closed squares) and ammonium sulfate (red closed circles)  $\sigma_{\omega_0}$  were obtained from Ferdousi Rokib et al., 2025 (in review). Sodium dodecyl sulfate (SDS)  $\sigma_{\omega_0}$  is shown as black diamonds. Pure water  $\sigma_{\omega_0}$  at 25°C (~72 mN m<sup>-1</sup>) is represented as a dashed blue line. Compounds can be categorized as weak to moderately surface active (65-65 mN m<sup>-1</sup>) or surface-active (surfactants, <65 mN m<sup>-1</sup>) for compounds that can depress surface tension below that of pure water. Bain et al 2023 consider the dilute bulk measurement regime to be less than 100mM.

tension values, > 72 mN m<sup>-1</sup> in the dilute regime. However, despite the presence of impurities in the mixture, synthesized 2-MTS <u>sample mixture</u> surface tension reaches values ~ 68 mN m<sup>-1</sup>. Therefore, the presence of these <u>additional compoundsimpurities</u> may counteract possible further surface tension depression exhibited by <u>pure 2-MTS</u>. Future <u>work can better probe</u> surface tension <u>modeling studies for synthesized of the pure organic</u> 2-MTS <u>data may be needed to probe the and effects of SMS</u> by <u>applying a multicomponent</u> surface <u>depressing abilities of the pure organosulfate component tension model</u> (e.g., multicomponent models of Topping et al., 2007). <u>to dynamic surface tension measurements</u>.

Both 2-MT and 2-MTS are considered viscous compounds and may diffuse slowly through the measured droplets (Reid et al., 2018; Zhang et al., 2019a; Chen et al., 2023). As a result, equilibrium surface tension is reached after a period of time, t. The rate of diffusion of the organic through water, also known as the diffusion coefficient Ds, can be calculated from dynamic surface tension measurements (Eq. 1-2). Diffusion coefficient values for synthesized 2-MT and 2-MTS samples range between 10<sup>-9</sup> to 10<sup>-11</sup> m<sup>2</sup> s<sup>-1</sup>, with diffusion slowing with increasing sample concentration. Specifically,  $D_s$  for the 2-MT and 2-MTS samples are estimated to be  $10^{-9}$  to  $10^{-11}$ m<sup>2</sup> s<sup>-1</sup> and 10<sup>-9</sup> to 10<sup>-10</sup> m<sup>2</sup> s<sup>-1</sup>, respectively (Table S17). Additionally, the viscosity-based diffusion coefficient was calculated and shown in Table S19. 2-MT and 2-MTS diffusion rates are comparable to rates observed for other previously investigated viscous components in aqueous solution (Curry et al., 2018; Tandon et al., 2019). For example, methylglyoxal, a known viscous component, has an aqueous phase diffusion rate ~ 10<sup>-9</sup> m<sup>-2</sup> s<sup>-1</sup> (Curry et al., 2018). In addition to the diffusion coefficients in aqueous solution, a study by Chenyakin et al. (2017) average diffusion coefficients between 10<sup>-13</sup> and 10<sup>-14</sup> m<sup>2</sup> s<sup>-1</sup> for organic molecules in a sucrose-water proxy for SOA. A study by Renbaum-Wolff et al. (2013) reported diffusion coefficients ranging from 10<sup>-13</sup> and 10<sup>-13</sup>  $^{15}$  m<sup>2</sup> s<sup>-1</sup> for  $\alpha$ -pinene-derived SOA between 70-90% RH. Indeed, 2-MT and 2-MTS have been previously observed to be highly viscous, resulting in slow diffusivity (Wang et al., 2011; Chenyakin et al., 2017; Tandon et al., 2019; Zhang et al., 2019a; Chen et al., 2023). Furthermore, at higher viscosity and lower diffusion rates, the diffusion of solute molecules fails to follow the Stokes-Einstein relationship describing the self-diffusion of solute molecules through a liquid phase (Einstein, 1905; Chenyakin et al., 2017; Tandon et al., 2019). For viscous material, such as 2-MT and 2-MTS sample, diffusion in water is self-limited (Chenyakin et al., 2017). Slow diffusion correlates with the longer time scales needed to reach equilibrium surface tension for more concentrated sample solutions; the solute molecules are limited in their ability to accumulate to the surface; thus, time is an important factor in the surface tension measurements. This effect is more prominent in 2-MT than 2-MTS sample, as evident in its slower diffusion rates for concentrations >30 mM (Table S17).

Formatted: Font: Italic

408

409

410

411

412

413 414

415

416

417 418

419

420

421

422

423

424

425

426

427

428

429

430 431

432

433

434 435

436 437

438

439

440

441 442

443 444 445

Previous studies have observed that inorganic compounds, such as AS, mixed with organics can enhance surface tension effects (Topping, 2010; El Haber et al., 2023). Additionally, AS can result in the partitioning of organics to the to the surface (i.e., the movement of organics to the surface is commonly referred to as salting-out). To determine if partitioning effects are present in organic/AS mixtures, <a href="mailto:synthesized">synthesized</a> 2-MT and 2-MTS <a href="mailto:samples">samples</a> were mixed with 500 mM AS and dynamic surface tension measurements were taken; mixture dynamic surface tension measurements are shown in Fig. 2. Average mixed surface tension values are listed in Table S10.

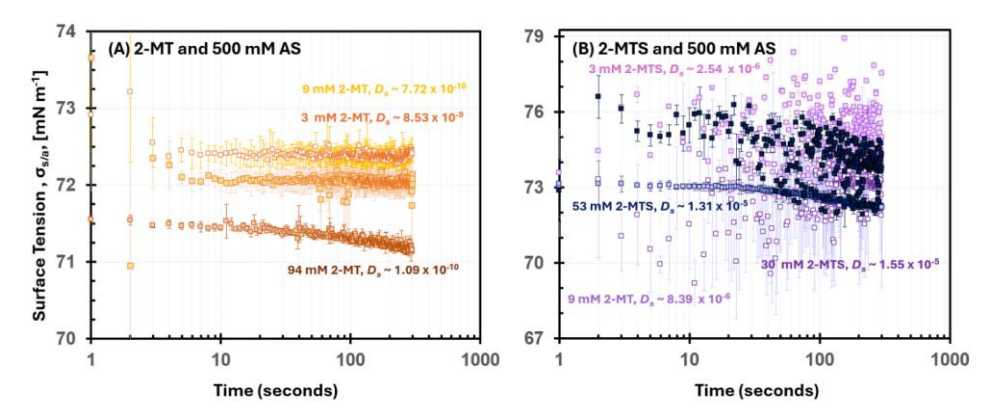


Figure 2. Dynamic σ<sub>s/a</sub> measurements for (A) 3–94 mM 2 MT/500 mM AS and (B) 3–53 mM 2 MTS/500 mM AS mixtures. Dynamic σ<sub>s/a</sub> was recorded over a duration of 300 seconds.

dynamic surface tension measurements and overall sample diffusivity.

For mixtures of 3-9 mM 2-MT and 500 mM AS, surface tension remains stable  $\sim$  75 mN m<sup>-1</sup> and is higher than pure-2-MT (>98 wt% purity) solution surface tension alone (Fig. 2A). Higher  $\sigma_{s/a}$  values indicate a lack of salting out effects and organic surface partitioning; previous surface tension studies of organic/AS mixtures observed salting out effects through lower  $\sigma_{s/a}$  values in comparison to pure organic solutions (Ferdousi-Rokib et al., 2025 (in review)). Thus, for 3-9 mM 2-MT with 500 mM AS mixtures, organic partitioning is not enhanced, and the droplet surface tension aligns with pure AS  $\sigma_{s/a}$  (Fig.1. and Table S16). When organic concentration in the mixture is increased to 94 mM, a stronger time dependence for surface tension is observed (Fig. 2A); an equilibrium surface tension of  $\sim$ 71.2 mN m<sup>-1</sup> is reached at  $\sim$ 300 s. This lower surface tension for 94 mM 2-MT with 500 mM AS compared to the previous 2-MT/AS mixture correlates with the higher concentration of organic in solution. However, the longer equilibrium time is indicative of a slow solute diffusion in the droplet.

Previous studies have observed diffusion effects within dynamic surface tension measurements and estimated solute diffusion (Eastoe et al., 1998; Bain et al., 2024). To determine organic diffusion within AS mixtures, the  $D_s$  was calculated using Eqs. 1-2. For 2-MT/AS mixtures,  $D_s$  ranged from  $10^{-9}$  to  $10^{-11}$ , with diffusion slowing as organic concentration increases (Fig. 2A, Table

S17). 2-MT organic diffusion in AS mixtures is similar to that of the pure organic 2-MT solution (with > 98% purity)  $D_s$  values. As a result, 2-MT organic diffusion remains relatively unaffected in the presence of AS. The organic 2-MT molecules do not diffuse fast enough to fully accumulate 473 at the surface and substantially lower surface tension.

Similar to 2-MT/AS mixtures, 2-MTS/AS mixture surface tension was higher than 2-MTS sample solution surface tension alone. 2-MTS/AS mixture  $\sigma_{s/a}$  values ranged from  $\sim 72.5$  to 75 mN m<sup>-1</sup> and remain close to surface tension values of pure AS. Furthermore,  $\sigma_{s/a}$  values remain constant as the 2-MTS organic concentration increases from 3 to 53 mM; the minimal correlation between organic concentration and surface tension implies that AS dominates droplet surface tension at the surface-air interface. In addition to being stable across organic concentrations. 2-MTS/AS  $\sigma_{s/a}$ reaches equilibrium faster than 2-MT/AS; equilibrium is achieved across the mixtures at < 100 s (Fig. 2B). Indeed, based on the dynamic surface tension measurements, Ds for 2-MTS within AS mixtures remains ~10<sup>-9</sup>, indicating slightly faster organic diffusivity through the droplet than 2-MT (Table S17). In the presence of AS, D<sub>s</sub> increases by an order of magnitude. This suggests the presence of AS increases solubility and dispersion of 2-MTS molecules through the droplet, (Prisle et al., 2010; Toivola et al., 2017). A similar phenomenon has been observed in glyoxal/AS mixtures as the presence of the inorganic compound improves dissolution of the organic (Kampf et al., 2013). Therefore, the higher 2-MTS/AS surface tension values and diffusivity indicate that the organic is well dispersed within the droplet, but AS dominates droplet surface tension properties. Both 2-MT and 2-MTS present complex viscous properties that may affect droplet phase and potentially change in the presence of inorganic compounds, such as AS. It is important to note that for 2-MTS, the remaining sample mass also contains SMS, which may further influence the estimated diffusion rates (Vignes, 1966; Guevara Carrion Wallace et al., 20162021). Future work should expand upon the methodology of this study to further understand the influence of SMS on viscous organic diffusivity, such as 2 MTS diffusion rates. Diffusion coefficients within aerosols may be sensitive to mixture ratio, as observed by Wallace et al. (2021). Thus, the presence of SMS may affect the 2-MTS sample/AS diffusion rates observed in this study. Future work should explore the influence of SMS on viscous organic diffusivity by applying this study's methodology to a range of 2-MTS sample/SMS mixtures with 2-MTS contribution greater than 73 wt%. Ultimately, diffusion effects were observed through dynamic surface tension measurements and may influence 2-MT, 2-MTS, and AS-mixed aerosol water uptake properties. Therefore, additional diffusion effects on synthesized organic and organic/AS aerosol mixtures were probed through the lens of water uptake measurements.

#### 4.2. Water Uptake Measurements

470

471

472

474

475

476

477

478

479

480

481

482

483 484

485

486

487

488

489

490

491 492

493 494

495

496

497

498

499 500

501

502

503 504

505

506

507

508

509

510

In addition to the previous measurements, the droplet growth of 2-MT, 2-MTS samples, and their respective AS mixtures were measured; hygroscopicity was estimated under both subsaturated and supersaturated conditions. Mixtures were varied by sample wt% (Table S21); organic wt% of 2-MTS is estimated by accounting for impurities present in the sample and their respective properties (e.g., density, hygroscopicity, Table S20). The adjusted mass wt% for 2-MTS/AS mixtures are listed in Table S21. For subsaturated hygroscopicity, the H-TDMA instrument setup was used to measure *G*<sub>F</sub> for all experimental solutions at 88.2% RH. Experimental growth factor values for 2-MT/AS and 2-MTS/AS mixtures are listed in Tables S20-S21. For supersaturated hygroscopicity, the CCNC instrument setup was used to obtain experimental *D*<sub>P,50</sub> values across multiple supersaturation conditions (0.31, 0.43, 0.65, 0.88, 1.10, 1.32, and 1.54 % SS); the critical diameter values for 2-MT/AS and 2-MTS/AS mixtures are listed in Tables S22-S23. For 100 wt% 2-MTS hygroscopicity, impurity (SMS and additional AS) hygroscopicity are accounted for by applying

517 ZSR mixing rule (Eq. 6) to solve for pure organic hygroscopicity; SMS κ was assumed to be ~0.459
 518 based on Peng et al. (2021).

519

520

521

522 523

524

525

526

527

528

Under subsaturated conditions, both 2-MT and 2-MTS are moderately hygroscopic, with  $\kappa_{\text{H-TDMA}}$  values of 0.103 and 0.276, respectively (Fig. 3A). For 2-MT/AS (Fig. 3A, orange open squares) and 2-MTS/AS (Fig. 3A, purple open circles) aerosol mixtures, subsaturated hygroscopicity values are similar. For 2-MT/AS mixtures  $\leq$  45 wt% organic,  $\kappa$  values plateau close to pure AS ( $\kappa_{\text{int}}$  = 0.61) at a  $\kappa_{\text{H-TDMA}} \sim 0.56$ . For mixtures  $\geq$  45 wt% organic, both 2-MT and 2-MTS exhibit lower  $\kappa_{\text{H-TDMA}}$  values, ranging from 0.103-0.505 for 2-MT/AS mixtures and 0.276–0.433 for 2-MTS/AS mixtures. Previous studies by Malek et al. (2023) and Ferdousi-Rokib et al. (in review) have observed a plateau in hygroscopicity for AS-dominated organic mixtures prior to a decrease in  $\kappa$  due to the presence of phase separated morphology; as a result of phase separation, the inorganic AS remains dissolved in the aqueous phase and drives

hygroscopicity (Malek et al., 2023). After a threshold composition is reached (45 wt% organic), more organic solute contributes to the aqueous phase and thus hygroscopicity is lowered.

Under supersaturated conditions, 2-MT and 2-MTS <u>samples</u> remain moderately hygroscopic, with  $\kappa_{\text{CCN}}$  being 0.269 and 0.139, respectively. For 2-MT/AS <u>sample</u> mixtures (Fig. 3B, closed orange

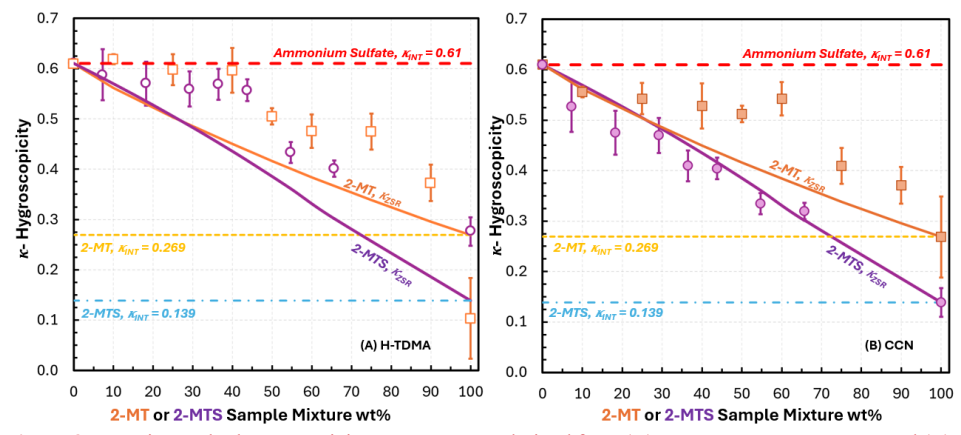


Figure 3. Experimental  $\kappa$  hygroscopicity measurements derived from (Λ) H TDMA measurements and (B) CCNC measurements. Subsaturated hygroscopicity ( $\kappa_{\rm H-TDMA}$ ) of 2-MT/AS and 2-MTS/AS mixtures are represented as open orange squares and open purple circles, respectively. Supersaturated hygroscopicity ( $\kappa_{\rm CCN}$ ) for 2 MT/AS and 2 MTS/AS mixtures are represented as orange squares and purple circles, respectively.  $\kappa$  Köhler theory ( $\kappa_{\rm ZSR}$ ) was used to predict hygroscopicity of 2 MT/AS (solid orange line) and 2 MTS/AS (solid purple line) via Eq. 6. Organic  $\kappa_{\rm int}$  was determined from 100 wt%  $\kappa_{\rm CCN}$ . 2 MT  $\kappa_{\rm int}$  (yellow dashed line) was determined to be 0.269. 2 MTS  $\kappa_{\rm int}$  (blue dashed line) was determined to be 0.139.

purple line) via Eq. 6. Organic  $\kappa_{int}$  was determined from 100 wt%  $\kappa_{CCN}$ . 2-MT  $\kappa_{int}$  (yellow dashed line) was determined to be 0.269. 2-MTS  $\kappa_{int}$  (blue dashed line) was determined to be 0.139.

squares), supersaturated  $\kappa$  mimics the same trend as subsaturated 2-MT/AS  $\kappa$ ; for mixtures  $\leq 60$  wt% 2-MT,  $\kappa_{CCN}$  also shows a plateau at  $\sim 0.53$  and then decreases with increased organic aerosol composition. In comparison, the 2-MTS/AS <u>sample</u> mixtures (Fig. 3B, purple circles) present a linear hygroscopic trend; as organic wt% increases,  $\kappa_{CCN}$  drops in a linear fashion resembling ideal mixing and volume additivity (Petters & Kreidenweis, 2007). Indeed, 2-MTS/AS  $\kappa_{CCN}$  correlates with the hygroscopicity trend predicted by  $\kappa_{ZSR}$  values (Eqs. 11-12) (Fig. 3B, purple line). 2-MTS/AS supersaturated hygroscopicity agrees well with original Köhler theory ( $R^2 = 0.972$ , Table S26), suggesting full 2-MTS dissolution and contribution to water uptake. By contrast, 2-MT/AS mixtures do not agree with  $\kappa$ -Köhler theory ( $R^2 = 0.787$ , Table S26), with the greatest discrepancy observed in the region between the  $\kappa$  experimental plateau and  $\kappa_{ZSR}$  (Fig. 3, orange line); additionally, subsaturated 2-MTS/AS mixtures deviate from  $\kappa_{ZSR}$  during the initial hygroscopic plateau (Fig. 3A, purple line). Thus, for 2-MT/AS mixtures and subsaturated 2-MTS/AS aerosols, the ideal volume additive mixing rule does not apply. This can once again be attributed to limitations to organic dissolution into the aqueous phase (Malek et al., 2023). For 2-MTS/AS

sample mixtures, both subsaturated and supersaturated hygroscopic trends may be further impacted by the presence by SMS. The contributions of AS and SMS hygroscopicity are accounted for 2-MTS sample mixture.  $\kappa$  was estimated using ZSR mixing rule, which assumes ideal interactions between SMS, AS, and 2-MTS. However, non-idealities (e.g., phase separation, salting in) may result in SMS having a greater influence on hygroscopicity and can be the focus of future exploration.

In addition to non-ideal hygroscopic trends, it is noted that overall,  $\kappa_{\rm CCN}$  values remain lower than  $\kappa_{\text{H-TDMA}}$  values for both 2-MT/AS and 2-MTS/AS sample mixtures, contrary to the usual trend of  $\kappa_{\rm CCN} > \kappa_{\rm H-TDMA}$  (Petters & Kreidenweis, 2007). The observed difference suggests greater organic dissolution and contribution to hygroscopicity in the supersaturated regime compared to subsaturated conditions. This suggests potential viscosity and diffusion limitations on hygroscopicity as RH transitions from sub- to supersaturated. Indeed, the viscosity of the 2-MT and 2-MTS changes under different conditions. Both compounds remain in the semi-solid phase state before entering the CCNC, and behave like liquids in the H-TDMA, as shown in Table S18. Additionally, Asa-Awuku and Nenes (2007) report diffusivity limitation effects on aerosol water uptake for compounds with  $D_s$  values  $\leq 2.5 \times 10^{-10}$ , well within the range of  $D_s$  values for 2-MT, and 2-MT sample/AS. Water uptake was shown to be driven by the viscous organic phase slowly diffusing into the aqueous phase (Asa-Awuku & Nenes, 2007). Thus, it is believed that both 2-MT and 2-MTS-organies slowly dissolve and phase separate to form a viscous phase under subsaturated conditions, corresponding to slow diffusion coefficients. AS is an inorganic compound that is assumed to instantaneously dissolve into the aqueous phase and thus drives hygroscopicity when the droplet is phase separated, such as for 2-MT/AS mixtures (Fig. 2). However, lower  $\kappa$  values at supersaturated conditions can be attributed to higher water content; previous studies have found greater water content correlating with reduced viscosity due to a plasticizing effect and resulting in enhanced organic mixing (O'Meara et al., 2016; Reid et al., 2018; Jeong et al., 2022). Thus, the organic viscous phase may experience "cracking" and greater movement of organic molecules through the aqueous phase (Tandon et al., 2019). Therefore, phase behavior of the organic can have a strong influence on aerosol water uptake. Additionally, the nonideal hygroscopic behavior of 2-MT/AS and subsaturated 2-MTS/AS mixtures versus the ideal hygroscopic behavior of supersaturated 2-MTS/AS aerosols can be probed through imaging of the aerosol mixture phase behavior.

#### 4.3. Phase Morphology

548

549

550

551

552 553

554

555

556

557

558

559

560 561

562

563 564

565 566

567 568

569

570 571

572

573

574 575

576

577

578 579 580

581

582 583

584

585

586

587

588

To further understand the phase state and morphology of 2-MT and 2-MTS <u>sample</u> mixtures with AS, AFM images were taken at varied organic wt% (Fig. 4). Dried synthesized 2-MTS presents itself as a viscous, spherical particle, indicated by its smooth surface (Fig. S4); this agrees with both shape factor measurement of ~1 (Armstrong et al., 2025 (2025)) and diffusion coefficient values. As inorganic AS is mixed with 2-MTS <u>sample</u>, phase behavior changes. At 10 wt% 2-MTS <u>sample</u> (Fig. 4B), particles exhibit an engulfed core-shell morphology. A previous study by Cooke et al. (2022) observed a similar core-shell morphology for AS-seeded IEPOX-derived SOA particles; the study observed an organic shell, while the inorganic salt was observed to be present

Formatted: Font: 16 pt

in the shell as well as within an aqueous core (Cooke et al., 2022). With AS dispersed on the outer shell as well as being present in an aqueous core, the inorganic salt in the shell will likely easily dissolve during water uptake and drive hygroscopicity, consistent with the results as observed in subsaturated hygroscopicity measurements. However, AS within the shell may introduce roughness in the outer edge which can promote "cracking" in the organic phase, which can result in full dissolution in the presence of higher water content and ideal mixing (Tandon et al., 2019).

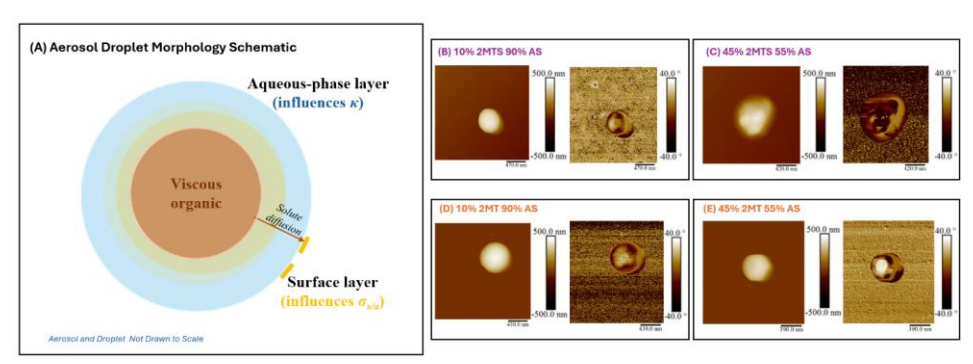


Figure 4. (A) Schematic depicting acrosol droplet composed of a viscous organic core and aqueous phase layer and AFM images of (B) 10 wt% 2 MTS 90 wt% AS (C) 45 wt% 2 MTS 55 wt% AS (D) 10 wt% 2 MT 90 wt% AS and (E) 45 wt% 2 MT 90 wt% AS. AFM results depict vertical particle height (left) and phase morphology (right).

As 2-MTS is increased to 45 wt%, the particle morphology shows greater inorganic phase dispersion, with AS protruding through the viscous organic phase (Fig. 4C). The visualized morphology and phase state of the particle agrees with behavior inferred from water-uptake and droplet measurements (Sect. 4.2). In particular, ~45 wt% is the observed threshold for the plateau in 2-MTS/AS  $\kappa_{\text{H-TDMA}}$  values, prior to a linear decrease in  $\kappa_{\text{H-TDMA}}$  values. The dispersion of AS disrupts the organic network within the viscous phase, giving rise to the observed roughness and promoting the salting in of 2-MTS. This phenomenon agrees with the results of previously published literature that show viscous organics mixed with AS; specifically, laboratory-generated SOA-AS and citric acid-AS mixtures (Saukko et al., 2012; Abramson et al., 2013). Previous studies have also observed increased diffusion within viscous SOA particles via a disruption of the hydrogen bonding network between the organic molecules that can promote solute movement in the droplet (Reid et al., 2018; Jeong et al., 2022; Sheldon et al., 2023). For this reason, it is likely that greater organic diffusion occurs above 45 wt% organic, resulting in decreasing  $\kappa_{\text{H-TDMA}}$  values. Furthermore, the well dispersed AFM morphology is indicative of ideal mixing under supersaturated conditions, thereby agreeing with  $\kappa$ -Köhler theory of droplet growth.

In comparison, 2-MT mixtures present an engulfed core-shell morphology from 10 to 45 wt% organic (Fig. 4D-E). At 10 wt% 2-MT, the viscous organic phase dominates the particle morphology and AS remains dispersed at the surface edge, as shown in Fig. 4D. As organic wt% increases to 45 wt%, morphology remains unchanged and the organic phase stays intact. The intact core-shell morphology of 45 wt% 2-MT aerosol mimic contrasts with the well dispersed

morphology observed for 45 wt% 2-MTS aerosol mimic. For 2-MT, the organic diffusion is limited under both sub- and supersaturated conditions, likely due to the undissolved viscous organic phase (Fig. 4A). Specifically, 2-MT viscosity causes slower dissolution compared to AS and results in the phase separated morphology. Thus, hygroscopicity of the 2-MT/AS mixture is dominated by AS dissolution from the core and outer shell, corresponding to the hygroscopic plateau observed for 2-MT/AS sub- and supersaturated water uptake measurements (Fig. 3). Therefore, particle morphology and viscosity influence the synthesized 2-MT's ability to diffuse through the aerosol droplet and can affect aerosol water uptake process. Indeed, a previous study by Zhang et al. (2018) described the "self-limiting" effect of a core-shell morphology on IEPOX-SOA reactive uptake and can now be observed in the 2-MT/AS water uptake process. However, diffusion limitations can also result in the need for longer time periods to reach an equilibrium state, as observed by dynamic surface tension measurements. Consequently, current hygroscopicity measurements that occur at fast time scales may not capture the full water uptake process of the synthesized organics and their mixtures. For example, the residence of aerosols within DMT CCNC columns is ~ 10 s (Paramonov et al., 2015) while similar H-TDMA instrument set ups have a residence time ~ 6.5 s (Mikhailov & Vlasenko, 2020). However, a previous study by Chuang et al. (2003) found atmospheric droplet growth timescales range between 5 to 100 s, congruent with the timescale of 2-MT and 2-MTS dynamic surface tension change (Fig. 2. and Chuang, 2003). Therefore, hygroscopicity of viscous organic containing aerosols, such as 2-MT and 2-MTS, must be studied at greater residence times to observe any possible effects on hygroscopicity; understanding whether timescale effects CCN activity of organic-inorganic aerosol mixtures can greatly impact current global models that may assume instantaneous solute dissolution during the water uptake process. Furthermore, future studies should consider whether the hygroscopicity approximations of viscous 2-MT/AS and 2-MTS/AS mixtures are time dependent, as time-dependent droplet formation has been observed for biogenic aerosols (Vizenor & Asa-Awuku, 2018). Currently, traditional  $\kappa$ -Köhler theory is unable to predict the water uptake of 2-MT/AS and subsaturated 2-MTS/AS aerosols and does not consider solute and droplet kinetic effects. However, by accounting for phase morphology and viscosity,  $\kappa$  predictions may be improved.

615

616

617

618

619

620

621 622

623

624

625

626

627

628 629

630

631 632

633

634

635 636

637

638

639 640

641

642 643

644

645

646

647

648

649

650

651

652 653

654

655

656

657

In addition, size-dependent morphology may also affect  $\kappa$ -hygroscopicity estimations. Several studies observe a relationship between particle size and aerosol phase transitions during water uptake (Veghte et al., 2013; Cheng et al., 2015; Altaf et al., 2016; Schmedding & Zuend, 2025). Specifically, Veghte et al. (2013) and Cheng et al. (2015) observe smaller AS-organic particles favoring a homogeneous liquid phase while larger particles remain in a partially engulfed morphology; this finding correlates with 2-MT/AS engulfed morphology for particles imaged  $\geq$  390 nm (Fig. 4). Indeed, for 2-MT/AS mixtures > 60 wt% 2-MT,  $\kappa_{\rm CCN}$  decreases with increasing dry activation diameter before plateauing (Fig. S5). This trend may correlate to greater organic diffusion as particle size and morphology changing before a dissolution limit is reached for > 60 wt% 2-MT/AS mixtures. For mixtures  $\leq$  60 wt% 2-MT, a similar decrease in  $\kappa_{\rm CCN}$  is observed before hygroscopicity begins to increase; this may be attributed to the engulfed morphology in larger particles (Fig. 4D-E) promoting AS dissolution and water uptake contribution while 2-MT diffusion reaches a limit. However, the water uptake measurements performed in this study do not account for size-dependent phase morphology in its analysis. Therefore, future work may build

upon the results of this study to better parameterize hygroscopicity based on initial particle size and size-dependent phase morphology affecting  $\kappa$ -hygroscopicity estimations. In particular, size-selected CCN measurements can be performed to better probe size-dependent morphology effects on aerosol activation. By doing so, global models can incorporate these influential physicochemical properties into predictions of aerosol-cloud interactions.

#### 5. Summary and Implications

In this study, we investigated the influence of solute diffusivity and droplet phase morphology on the hygroscopicity of synthesized 2-MT\_sample, 2-MTS\_sample, and their mixtures with AS. Mixtures with AS were varied by organic wt%. Both 2-MT and 2-MTS were previously observed to be viscous and glassy, affecting diffusivity through water. Additionally, previous studies found 2-MT to be weakly surface-active. To determine organic diffusivity and potential surface activity, dynamic surface tension measurements were taken for aqueous organic and mixed organicinorganic solutions. 2-MT and 2-MTS were found to be weakly surface-active. Previous studies by Bain et al., 2023 and Mikhailov et al., 2024 determined that surface activity in the dilute bulk concentration range correlates with depressed aerosol surface tension. However, neither 2-MT sample nor 2-MTS sample are sufficiently surface-active to depress droplet surface tension at the air-surface interface, 2-MT and 2-MTS sample solutes move slowly in droplets and have estimated diffusion rates (D<sub>s</sub>) between 10<sup>-9</sup> to 10<sup>-11</sup> m<sup>2</sup> s<sup>-1</sup>, with diffusion slowing as organic concentration is increased. When mixed with AS, 2-MT diffusivity remains slow (10<sup>-10</sup> m<sup>2</sup> s<sup>-1</sup>) while 2-MTS diffusivity increases by an order of magnitude (10<sup>-9</sup> m<sup>2</sup> s<sup>-1</sup>); 2-MTS diffusion in aqueous ASmixtures is similar to other quickly dissolving compounds, such as NaCl ( $D_s = 10^{-9}$ , Vitagliano & Lyons, 1956; Leaist & Hao, 1992) and can result in a well-mixed droplet.

-Organic viscosity and diffusion have have been shown to affect aerosol water uptake (Asa-Awuku & Nenes, 2007; Bones et al., 2012; Tandon et al., 2019). For 2-MT, 2-MTS sample, and subsequent mixtures under both sub- and supersaturated conditions, droplet growth is affected by solute diffusion. Subsaturated droplet growth was measured using a H-TDMA at 88.2% RH and subsaturated hygroscopicity was parameterized by  $\kappa_{\text{H-TDMA}}$ . For supersaturated conditions, a CCNC determined the activation ratio of particles at varied supersaturations (0.3-1.4% SS) and water uptake was parameterized by  $\kappa_{\text{CCN}}$ . 2-MT/AS mixtures exhibit plateaued  $\kappa_{\text{H-TDMA}}$  and  $\kappa_{\text{CCN}}$  values close to  $\kappa_{\text{int}}$  of AS (~0.61). A similar plateau behavior is observed for 2-MTS/AS  $\kappa_{\text{H-TDMA}}$ . However, for supersaturated conditions, 2-MTS/AS mixture  $\kappa_{\text{CCN}}$  follows ideal mixing behavior, represented by its proximity to  $\kappa$ -hygroscopicity predicted by  $\kappa$ -Köhler theory and volume additive ZSR. Additionally,  $\kappa_{\text{H-TDMA}}$  remains higher than  $\kappa_{\text{CCN}}$ ; this is a result of increased water content reducing viscosity effects and enhancing organic dissolution under supersaturated conditions.

The κ-hygroscopicity plateau in Fig. 3 has been previously attributed to the presence of phase separation, resulting in the inorganic, more soluble, and ideal compound (AS) driving water uptake (Malek et al., 2023). However, for 2-MTS\_/AS ideal hygroscopic behavior is indicative of a well dissolved, homogeneous droplet (Petters & Kreidenweis, 2007). To better understand phase morphology of the synthesized organic-AS mixed particles, AFM measurements of synthesized 2-MTS, 2-MTS/AS mixtures, and 2-MT/AS mixtures were acquired. 2-MTS aerosols are smooth, spherical, viscous particles; when mixed with AS at 10 wt%, AS remains in the aqueous core and

is dispersed on the side of the particle, introducing roughness on the aerosol outer shell. As organic concentration increases, the AS core is broken up through the particle. The less defined core-shell morphology may be the result of AS disrupting the interactions between neighboring 2-MTS particles in the viscous network; as a result, organic dissolution becomes faster as indicated by greater 2-MTS diffusion rates. Thus, 2-MTS sample/AS aerosols behave similar to traditional full dissolution assumptions. In comparison, 2-MT/AS mixture AFM images show an engulfed coreshell morphology regardless of organic concentration. As a result, the viscous organic phase remains intact while aqueous AS in the core drives hygroscopicity. A caveat to these results is the presence of SMS, an organosulfate, being present within the 2-MTS sample at ~24 wt%. Therefore, SMS may have an effect on surface tension, diffusivity, and hygroscopic trends observed for the 2-MTS sample/AS mixtures that is currently unknown in this study. Future work may utilize the methodology laid out in this work to more deeply probe the influence of SMS and any additional mixture component on viscous organic properties and water uptake.

699

700

701

702 703

704

705

706

707

708

709

710

711

712 713

714

715

716

717

718 719

720 721

722

723

724

725 726

727

728

729 730

731

732

733

734

735 736

737

738

739

740

741

This study demonstrates that viscosity can dictate organic diffusion through aqueous droplets, resulting in complex phase morphology and water uptake properties. IndeedFurthermore, the synthesized samples studied in this work a representative of the hygroscopic properties of IEPOX-SOA mixtures. A recent study by Armstrong et al. (2025) determined that the IEPOX-SOA composition is composed of a range of 2-MT, 2-MTS, and additional components that vary with aerosol acidity. Thus, the synthesized samples present in this work may present a subset of SOA aerosols generated and this study provides insight into its potential diffusive, hygroscopic, and phase behavior. For example, as shown by this study's water uptake measurements, hygroscopicity from the subsaturated to supersaturated regime evolves due to the presence of increased water content. However, it is also noted that the hygroscopicity measurements performed in this study were on short time scales (6-10 s); in comparison, dynamic surface tension measurements showed droplet equilibrium being reached at 100-300 s for aqueous 2-MT, 2-MT/AS, and 2-MTS. Thus, current water uptake measurements may not capture a potentially evolving hygroscopicity over time. This is critical in understanding biogenic aerosol influence on cloud formation; a previous study by Chuang (2003) found that droplet formation can occur within time scales of 5-100 s, well within evolving diffusion times observed in this study. Therefore, future work must investigate potentially dynamic water uptake of viscous biogenic aerosols, such as 2-MT, 2-MTS. Furthermore, time dependent  $\kappa$  can be developed to better account for organic diffusion within larger scale cloud parcel and global models. In addition to time dependency,  $\kappa$ -hygroscopicity estimations may also be affected by size dependent phase morphology. A study by Veghte et al. (2013) found smaller aerosol particles preferring a homogenous state, while larger particles have an engulfed core-shell morphology similar to 2-MT/AS aerosols in this study. Therefore, particle size may influence viscous organic-AS water uptake due to diffusion and morphological influences. Future work may explore and parameterize the effect of size-dependent phase separated morphology on aerosol activation through step size-selected CCN measurements. Ultimately, it is crucial to understand how biogenic aerosols, such as 2-MT and 2-MTS, properties (viscosity, diffusivity, and phase morphology) alter cloud formation. The results of this study demonstrate the co-dependency of these properties for two isoprene derived compounds and thus may improve our overall understanding of how biogenic aerosols, and their mixtures affect aerosol-cloud interactions.

743 Author Contributions: NF designed, collected, analyzed all experimental data, and analyzed 744 theoretical models. CA contributed to design and analysis of water uptake data. SJ contributed to 745 design and collection of H-TDMA experimental data. AD contributed to design and analysis of AFM data. MA contributed to design and collection of AFM data. ERR contributed to collection 746 747 of surface tension experimental data. ZZ and AG contributed to sample synthesis. JLW contributed 748 to design, collection, and analysis of dynamic surface tension experimental data. YZ contributed 749 to viscosity, diffusion, and AFM data analysis. All authors contributed to the writing and 750 preparation of the manuscript. 751 Competing Interest Statement: The authors have no competing interests to declare 752 753 **Acknowledgements:** The authors acknowledge the support of this work by NSF under AGS #2131369, AGS #2124489, 754 755 AGS #2131369 (Y.Z.), AGS #2131370 (J.S.), and AGS #2304669 (A.G., Z.Z., J.D.S.). 756 The authors acknowledge the characterization part of this work was performed in Texas A&M University Materials Characterization Core Facility (RRID:SCR 022202). 757 758 759 760 761 762 Abramson, E., Imre, D., Beránek, J., Wilson, J., & Zelenyuk, A. (2013). Experimental determination of 763 chemical diffusion within secondary organic aerosol particles [10.1039/C2CP44013J]. 764 Physical Chemistry Physics, 2983-2991. Chemical 15(8), https://doi.org/10.1039/C2CP44013J 765 766 Albrecht, B. A. (1989). Aerosols, Cloud Microphysics, and Fractional Cloudiness. Science, 767 245(4923), 1227-1230. https://doi.org/doi:10.1126/science.245.4923.1227 768 Altaf, M. B., Zuend, A., & Freedman, M. A. (2016). Role of nucleation mechanism on the size 769 dependent morphology of organic aerosol [10.1039/C6CC03826C]. 770 Communications, 52(59), 9220-9223. https://doi.org/10.1039/C6CC03826C 771 Armstrong, N. C., Gagan, S., Dodero, A. J., Ferdousi-Rokib, N., Frauenheim, M., Gold, A., Zhang, Z., 772 Asa-Awuku, A., Zhang, Y., & Surratt, J. D. (2025). Hygroscopicity Depends on Aerosol Acidity 773 and Sulfate Content during the Reactive Uptake of Isoprene Epoxydiols. ACS Earth and 774 Space Chemistry. https://doi.org/10.1021/acsearthspacechem.5c00163 Asa-Awuku, A., & Nenes, A. (2007). Effect of solute dissolution kinetics on cloud droplet formation: 775 776 Extended Köhler theory. Journal of Geophysical Research: Atmospheres, 112(D22). 777 https://doi.org/https://doi.org/10.1029/2005JD006934

Bain, A., Ghosh, K., Prisle, N. L., & Bzdek, B. R. (2023). Surface-Area-to-Volume Ratio Determines

9(11), 2076-2083. https://doi.org/10.1021/acscentsci.3c00998

Surface Tensions in Microscopic, Surfactant-Containing Droplets. ACS Central Science,

742

778

779

780

Formatted: Font: Times New Roman, 12 pt

Formatted: Justified
Formatted: Font: Bold

Bain, A., Lalemi, L., Croll Dawes, N., Miles, R. E. H., Prophet, A. M., Wilson, K. R., & Bzdek, B. R.
 (2024). Surfactant Partitioning Dynamics in Freshly Generated Aerosol Droplets. *Journal of the American Chemical Society*, 146(23), 16028–16038.
 https://doi.org/10.1021/jacs.4c03041

- Beier, T., Cotter, E. R., Galloway, M. M., & Woo, J. L. (2019). In Situ Surface Tension Measurements of Hanging Droplet Methylglyoxal/Ammonium Sulfate Aerosol Mimics under Photooxidative Conditions. ACS Earth and Space Chemistry, 3(7), 1208–1215. https://doi.org/10.1021/acsearthspacechem.9b00123
- Bertram, A. K., Martin, S. T., Hanna, S. J., Smith, M. L., Bodsworth, A., Chen, Q., Kuwata, M., Liu, A., You, Y., & Zorn, S. R. (2011). Predicting the relative humidities of liquid-liquid phase separation, efflorescence, and deliquescence of mixed particles of ammonium sulfate, organic material, and water using the organic-to-sulfate mass ratio of the particle and the oxygen-to-carbon elemental ratio of the organic component. *Atmos. Chem. Phys.*, *11*(21), 10995–11006. https://doi.org/10.5194/acp-11-10995-2011
- Bondy, A. L., Bonanno, D., Moffet, R. C., Wang, B., Laskin, A., & Ault, A. P. (2018). The diverse chemical mixing state of aerosol particles in the southeastern United States. *Atmos. Chem. Phys.*, *18*(16), 12595–12612. <a href="https://doi.org/10.5194/acp-18-12595-2018">https://doi.org/10.5194/acp-18-12595-2018</a>
- Bones, D. L., Reid, J. P., Lienhard, D. M., & Krieger, U. K. (2012). Comparing the mechanism of water condensation and evaporation in glassy aerosol. *Proceedings of the National Academy of Sciences*, 109(29), 11613–11618. https://doi.org/doi:10.1073/pnas.1200691109
- Chan, M. N., Surratt, J. D., Claeys, M., Edgerton, E. S., Tanner, R. L., Shaw, S. L., Zheng, M., Knipping, E. M., Eddingsaas, N. C., Wennberg, P. O., & Seinfeld, J. H. (2010). Characterization and Quantification of Isoprene-Derived Epoxydiols in Ambient Aerosol in the Southeastern United States. *Environmental Science & Technology*, 44(12), 4590–4596. https://doi.org/10.1021/es100596b
- Chen, B., Mirrielees, J. A., Chen, Y., Onasch, T. B., Zhang, Z., Gold, A., Surratt, J. D., Zhang, Y., & Brooks, S. D. (2023). Glass Transition Temperatures of Organic Mixtures from Isoprene Epoxydiol-Derived Secondary Organic Aerosol. *The Journal of Physical Chemistry A*, 127(18), 4125–4136. https://doi.org/10.1021/acs.jpca.2c08936
- Chen, Y., Dombek, T., Hand, J., Zhang, Z., Gold, A., Ault, A. P., Levine, K. E., & Surratt, J. D. (2021). Seasonal Contribution of Isoprene-Derived Organosulfates to Total Water-Soluble Fine Particulate Organic Sulfur in the United States. ACS Earth and Space Chemistry, 5(9), 2419–2432. https://doi.org/10.1021/acsearthspacechem.1c00102
- Cheng, Y., Su, H., Koop, T., Mikhailov, E., & Pöschl, U. (2015). Size dependence of phase transitions in aerosol nanoparticles. *Nature Communications*, 6(1), 5923. https://doi.org/10.1038/ncomms6923
- Chenyakin, Y., Ullmann, D. A., Evoy, E., Renbaum-Wolff, L., Kamal, S., & Bertram, A. K. (2017). Diffusion coefficients of organic molecules in sucrose–water solutions and comparison with Stokes–Einstein predictions. *Atmos. Chem. Phys.*, 17(3), 2423–2435. <a href="https://doi.org/10.5194/acp-17-2423-2017">https://doi.org/10.5194/acp-17-2423-2017</a>
- Chernyshev, V. S., & Skliar, M. (2015). Diffusivity Measurements of Solutes Impacting Interfacial
   Tension. Industrial & Engineering Chemistry Research, 54(16), 4535–4544.
   https://doi.org/10.1021/ie504355w
- Chuang, P. Y. (2003). Measurement of the timescale of hygroscopic growth for atmospheric aerosols. *Journal of Geophysical Research: Atmospheres*, 108(D9). https://doi.org/https://doi.org/10.1029/2002JD002757
- Claeys, M., Graham, B., Vas, G., Wang, W., Vermeylen, R., Pashynska, V., Cafmeyer, J., Guyon, P.,
   Andreae, M. O., Artaxo, P., & Maenhaut, W. (2004). Formation of Secondary Organic Aerosols

- 829 Through Photooxidation of Isoprene. *Science*, *303*(5661), 1173–1176. 830 <a href="https://doi.org/doi:10.1126/science.1092805">https://doi.org/doi:10.1126/science.1092805</a>
- Cooke, M. E., Armstrong, N. C., Lei, Z., Chen, Y., Waters, C. M., Zhang, Y., Buchenau, N. A., Dibley,
   M. Q., Ledsky, I. R., Szalkowski, T., Lee, J. Y., Baumann, K., Zhang, Z., Vizuete, W., Gold, A.,
   Surratt, J. D., & Ault, A. P. (2022). Organosulfate Formation in Proxies for Aged Sea Spray
   Aerosol: Reactive Uptake of Isoprene Epoxydiols to Acidic Sodium Sulfate. ACS Earth and
   Space Chemistry, 6(12), 2790–2800. https://doi.org/10.1021/acsearthspacechem.2c00156

- Curry, L. A., Tsui, W. G., & McNeill, V. F. (2018). Technical note: Updated parameterization of the reactive uptake of glyoxal and methylglyoxal by atmospheric aerosols and cloud droplets. *Atmos. Chem. Phys.*, *18*(13), 9823–9830. https://doi.org/10.5194/acp-18-9823-2018
- Cziczo, D. J., Nowak, J. B., Hu, J. H., & Abbatt, J. P. D. (1997). Infrared spectroscopy of model tropospheric aerosols as a function of relative humidity: Observation of deliquescence and crystallization. *Journal of Geophysical Research: Atmospheres*, 102(D15), 18843–18850. https://doi.org/https://doi.org/10.1029/97JD01361
- DeCarlo, P. F., Slowik, J. G., Worsnop, D. R., Davidovits, P., & Jimenez, J. L. (2004). Particle Morphology and Density Characterization by Combined Mobility and Aerodynamic Diameter Measurements. Part 1: Theory. Aerosol Science and Technology, 38(12), 1185–1205. https://doi.org/10.1080/027868290903907
- DeRieux, W. S. W., Li, Y., Lin, P., Laskin, J., Laskin, A., Bertram, A. K., Nizkorodov, S. A., & Shiraiwa, M. (2018). Predicting the glass transition temperature and viscosity of secondary organic material using molecular composition. *Atmos. Chem. Phys.*, 18(9), 6331–6351. <a href="https://doi.org/10.5194/acp-18-6331-2018">https://doi.org/10.5194/acp-18-6331-2018</a>
- Eastoe, J., Dalton, J. S., Rogueda, P. G. A., & Griffiths, P. C. (1998). Evidence for Activation–Diffusion Controlled Dynamic Surface Tension with a Nonionic Surfactant. *Langmuir*, *14*(5), 979–981. https://doi.org/10.1021/la971241w
- Einstein, A. (1905). Über die von der molekularkinetischen Theorie der Wärme geforderte Bewegung von in ruhenden Flüssigkeiten suspendierten Teilchen. *Annalen der Physik*, *322*(8), 549–560. https://doi.org/https://doi.org/10.1002/andp.19053220806
- El Haber, M., Ferronato, C., Giroir-Fendler, A., Fine, L., & Nozière, B. (2023). Salting out, non-ideality and synergism enhance surfactant efficiency in atmospheric aerosols. *Scientific Reports*, 13(1), 20672. https://doi.org/10.1038/s41598-023-48040-5
- Ferdousi-Rokib, N., A. Malek, K., Mitchell, I., M. Fierce, L., & Asa-Awuku, A. A. (2025). Aerosol Hygroscopicity and Surface-Active Coverage for the Droplet Growth of Aerosol Mixtures. ACS ES&TAir, 2(8), 1454–1467. https://doi.org/10.1021/acsestair.4c00303
- Fertil, D., Pierre-Louis, K., Ingwer, S., Galloway, M. M., & Woo, J. L. (2025). Surfactant Effects in Irradiated, Hanging-Droplet, Aqueous-Phase Glyoxal/Ammonium Sulfate Aerosol Mimic Systems. ACS Earth and Space Chemistry. https://doi.org/10.1021/acsearthspacechem.4c00288
- Fordham, S., & Freeth, F. A. (1948). On the calculation of surface tension from measurements of pendant drops. *Proceedings of the Royal Society of London. Series A. Mathematical and Physical Sciences*, 194(1036), 1–16. https://doi.org/doi:10.1098/rspa.1948.0063
- Freedman, M. A. (2017). Phase separation in organic aerosol [10.1039/C6CS00783J]. *Chemical Society Reviews*, 46(24), 7694–7705. https://doi.org/10.1039/C6CS00783J
- Froyd, K. D., Murphy, S. M., Murphy, D. M., de Gouw, J. A., Eddingsaas, N. C., & Wennberg, P. O.
   (2010). Contribution of isoprene-derived organosulfates to free tropospheric aerosol mass.
   Proceedings of the National Academy of Sciences, 107(50), 21360–21365.
   https://doi.org/doi:10.1073/pnas.1012561107

- Fuchs, N. A. (1963). On the stationary charge distribution on aerosol particles in a bipolar ionic atmosphere. *Geofisica pura* e applicata, 56(1), 185–193. https://doi.org/10.1007/BF01993343
- 879 Gohil, K. (2022). kgohil27/PyCAT: v1.0 (v1.0). Zenodo.

- Gohil, K., & Asa-Awuku, A. A. (2022). Cloud condensation nuclei (CCN) activity analysis of low-hygroscopicity aerosols using the aerodynamic aerosol classifier (AAC). Atmos. Meas. Tech.,
   15(4), 1007–1019. https://doi.org/10.5194/amt-15-1007-2022
  - Guenther, A. B., Jiang, X., Heald, C. L., Sakulyanontvittaya, T., Duhl, T., Emmons, L. K., & Wang, X. (2012). The Model of Emissions of Gases and Aerosols from Nature version 2.1 (MEGAN2.1): an extended and updated framework for modeling biogenic emissions. *Geosci. Model Dev.*, 5(6), 1471–1492. https://doi.org/10.5194/gmd-5-1471-2012
  - Guevara-Carrion, G., Gaponenko, Y., Janzen, T., Vrabec, J., & Shevtsova, V. (2016). Diffusion in Multicomponent Liquids: From Microscopic to Macroscopic Scales. *The Journal of Physical Chemistry B.* 120(47), 12193–12210. https://doi.org/10.1021/acs.ipcb.6b09810
  - Hettiyadura, A. P. S., Al-Naiema, I. M., Hughes, D. D., Fang, T., & Stone, E. A. (2019). Organosulfates in Atlanta, Georgia: anthropogenic influences on biogenic secondary organic aerosol formation. Atmos. Chem. Phys., 19(5), 3191–3206. <a href="https://doi.org/10.5194/acp-19-3191-2019">https://doi.org/10.5194/acp-19-3191-2019</a>
  - Hughes, D. D., Christiansen, M. B., Milani, A., Vermeuel, M. P., Novak, G. A., Alwe, H. D., Dickens, A.
    F., Pierce, R. B., Millet, D. B., Bertram, T. H., Stanier, C. O., & Stone, E. A. (2021). PM2.5 chemistry, organosulfates, and secondary organic aerosol during the 2017 Lake Michigan Ozone Study. Atmospheric Environment, 244, 117939. https://doi.org/https://doi.org/10.1016/j.atmosenv.2020.117939
  - Hyvärinen, A.-P., Raatikainen, T., Laaksonen, A., Viisanen, Y., & Lihavainen, H. (2005). Surface tensions and densities of H2SO4 + NH3 + water solutions. *Geophysical Research Letters*, 32(16). https://doi.org/https://doi.org/10.1029/2005GL023268
  - Intergovernmental Panel on Climate, C. (2023). Climate Change 2021 The Physical Science Basis:

    Working Group I Contribution to the Sixth Assessment Report of the Intergovernmental Panel
    on Climate Change. Cambridge University Press. <a href="https://doi.org/DOI:10.1017/9781009157896">https://doi.org/DOI:10.1017/9781009157896</a>
  - Jeong, R., Lilek, J., Zuend, A., Xu, R., Chan, M. N., Kim, D., Moon, H. G., & Song, M. (2022). Viscosity and physical state of sucrose mixed with ammonium sulfate droplets. *Atmos. Chem. Phys.*, 22(13), 8805–8817. https://doi.org/10.5194/acp-22-8805-2022
  - Joos, P., & Rillaerts, E. (1981). Theory on the determination of the dynamic surface tension with the drop volume and maximum bubble pressure methods. *Journal of Colloid and Interface Science*, 79(1), 96–100. https://doi.org/https://doi.org/10.1016/0021-9797(81)90051-5
  - Kampf, C. J., Waxman, E. M., Slowik, J. G., Dommen, J., Pfaffenberger, L., Praplan, A. P., Prévôt, A. S. H., Baltensperger, U., Hoffmann, T., & Volkamer, R. (2013). Effective Henry's Law Partitioning and the Salting Constant of Glyoxal in Aerosols Containing Sulfate. *Environmental Science & Technology*, 47(9), 4236–4244. <a href="https://doi.org/10.1021/es400083d">https://doi.org/10.1021/es400083d</a>
  - Kanakidou, M., Seinfeld, J. H., Pandis, S. N., Barnes, I., Dentener, F. J., Facchini, M. C., Van Dingenen, R., Ervens, B., Nenes, A., Nielsen, C. J., Swietlicki, E., Putaud, J. P., Balkanski, Y., Fuzzi, S., Horth, J., Moortgat, G. K., Winterhalter, R., Myhre, C. E. L., Tsigaridis, K., . . . Wilson, J. (2005). Organic aerosol and global climate modelling: a review. *Atmos. Chem. Phys.*, 5(4), 1053–1123. https://doi.org/10.5194/acp-5-1053-2005
- Kang, B., Tang, H., Zhao, Z., & Song, S. (2020). Hofmeister Series: Insights of Ion Specificity from
   Amphiphilic Assembly and Interface Property. ACS Omega, 5(12), 6229–6239.
   https://doi.org/10.1021/acsomega.0c00237

Kleinheins, J., Shardt, N., Lohmann, U., & Marcolli, C. (2025). The surface tension and cloud
 condensation nuclei (CCN) activation of sea spray aerosol particles. *Atmos. Chem. Phys.*,
 25(2), 881–903. https://doi.org/10.5194/acp-25-881-2025

- Köhler, H. (1936). The nucleus in and the growth of hygroscopic droplets [10.1039/TF9363201152].

  Transactions of the Faraday Society, 32(0), 1152–1161.

  https://doi.org/10.1039/TF9363201152
- Kreidenweis, S. M., & Asa-Awuku, A. (2014). 5.13 Aerosol Hygroscopicity: Particle Water Content and Its Role in Atmospheric Processes. In H. D. Holland & K. K. Turekian (Eds.), *Treatise on Geochemistry (Second Edition)* (pp. 331–361). Elsevier. https://doi.org/https://doi.org/10.1016/B978-0-08-095975-7.00418-6
  - Lance, S., Nenes, A., Medina, J., & Smith, J. N. (2006). Mapping the Operation of the DMT Continuous Flow CCN Counter. *Aerosol Science and Technology*, 40(4), 242–254. https://doi.org/10.1080/02786820500543290
  - Laskina, O., Morris, H. S., Grandquist, J. R., Qin, Z., Stone, E. A., Tivanski, A. V., & Grassian, V. H. (2015). Size Matters in the Water Uptake and Hygroscopic Growth of Atmospherically Relevant Multicomponent Aerosol Particles. *The Journal of Physical Chemistry A*, 119(19), 4489–4497. https://doi.org/10.1021/jp510268p
  - Leaist, D. G., & Hao, L. (1992). Binary mutual diffusion coefficients of aqueous ammonium and potassium sulfates at 25°C. *Journal of Solution Chemistry*, 21(4), 345–350. https://doi.org/10.1007/BF00647857
  - Malek, K., Gohil, K., Olonimoyo, E. A., Ferdousi-Rokib, N., Huang, Q., Pitta, K. R., Nandy, L., Voss, K. A., Raymond, T. M., Dutcher, D. D., Freedman, M. A., & Asa-Awuku, A. (2023). Liquid–Liquid Phase Separation Can Drive Aerosol Droplet Growth in Supersaturated Regimes. ACS Environmental Au. https://doi.org/10.1021/acsenvironau.3c00015
  - Mikhailov, E. F., & Vlasenko, S. S. (2020). High-humidity tandem differential mobility analyzer for accurate determination of aerosol hygroscopic growth, microstructure, and activity coefficients over a wide range of relative humidity. *Atmos. Meas. Tech.*, 13(4), 2035–2056. https://doi.org/10.5194/amt-13-2035-2020
  - Mikhailov, E. F., Vlasenko, S. S., & Kiselev, A. A. (2024). Water activity and surface tension of aqueous ammonium sulfate and D-glucose aerosol nanoparticles. *Atmos. Chem. Phys.*, 24(5), 2971–2984. https://doi.org/10.5194/acp-24-2971-2024
  - Moore, R. H., Nenes, A., & Medina, J. (2010). Scanning Mobility CCN Analysis—A Method for Fast Measurements of Size-Resolved CCN Distributions and Activation Kinetics. *Aerosol Science* and Technology, 44(10), 861–871. <a href="https://doi.org/10.1080/02786826.2010.498715">https://doi.org/10.1080/02786826.2010.498715</a>
  - Murphy, D. M., Thomson, D. S., & Mahoney, M. J. (1998). In Situ Measurements of Organics, Meteoritic Material, Mercury, and Other Elements in Aerosols at 5 to 19 Kilometers. Science, 282(5394), 1664–1669. https://doi.org/doi:10.1126/science.282.5394.1664
  - O'Meara, S., Topping, D. O., & McFiggans, G. (2016). The rate of equilibration of viscous aerosol particles. *Atmos. Chem. Phys.*, 16(8), 5299–5313. https://doi.org/10.5194/acp-16-5299-2016
  - Ott, E.-J. E., Tackman, E. C., & Freedman, M. A. (2020). Effects of Sucrose on Phase Transitions of Organic/Inorganic Aerosols. ACS Earth and Space Chemistry, 4(4), 591–601. https://doi.org/10.1021/acsearthspacechem.0c00006
- Padró, L. T., Tkacik, D., Lathem, T., Hennigan, C. J., Sullivan, A. P., Weber, R. J., Huey, L. G., & Nenes, A. (2010). Investigation of cloud condensation nuclei properties and droplet growth kinetics of the water-soluble aerosol fraction in Mexico City. *Journal of Geophysical Research: Atmospheres*, 115(D9). https://doi.org/https://doi.org/10.1029/2009JD013195

Paramonov, M., Kerminen, V. M., Gysel, M., Aalto, P. P., Andreae, M. O., Asmi, E., Baltensperger, U.,
 Bougiatioti, A., Brus, D., Frank, G. P., Good, N., Gunthe, S. S., Hao, L., Irwin, M., Jaatinen, A.,
 Jurányi, Z., King, S. M., Kortelainen, A., Kristensson, A., . . . Sierau, B. (2015). A synthesis of
 cloud condensation nuclei counter (CCNC) measurements within the EUCAARI network.
 Atmos. Chem. Phys., 15(21), 12211–12229. https://doi.org/10.5194/acp-15-12211-2015

- Paulot, F., Crounse, J. D., Kjaergaard, H. G., Kürten, A., St. Clair, J. M., Seinfeld, J. H., & Wennberg, P. O. (2009). Unexpected Epoxide Formation in the Gas-Phase Photooxidation of Isoprene. Science, 325(5941), 730–733. https://doi.org/doi:10.1126/science.1172910
- Peng, C., Razafindrambinina, P. N., Malek, K. A., Chen, L., Wang, W., Huang, R. J., Zhang, Y., Ding, X., Ge, M., Wang, X., Asa-Awuku, A. A., & Tang, M. (2021). Interactions of organosulfates with water vapor under sub- and supersaturated conditions. *Atmos. Chem. Phys.*, 21(9), 7135–7148. https://doi.org/10.5194/acp-21-7135-2021
- Petters, M. D., & Kreidenweis, S. M. (2007). A single parameter representation of hygroscopic growth and cloud condensation nucleus activity. *Atmos. Chem. Phys.*, 7(8), 1961–1971. https://doi.org/10.5194/acp-7-1961-2007
- Pratt, K. A., & Prather, K. A. (2010). Aircraft measurements of vertical profiles of aerosol mixing states. *Journal of Geophysical Research: Atmospheres*, 115(D11). https://doi.org/https://doi.org/10.1029/2009JD013150
- Prisle, N., & Mølgaard, B. (2018). Modeling CCN activity of chemically unresolved model HULIS, including surface tension, non-ideality, and surface partitioning. *Atmospheric Chemistry and Physics Discussions*, 1–23. https://doi.org/10.5194/acp-2018-789
- Prisle, N. L., Engelhart, G. J., Bilde, M., & Donahue, N. M. (2010). Humidity influence on gas-particle phase partitioning of α-pinene + O3 secondary organic aerosol. *Geophysical Research Letters*, 37(1). https://doi.org/https://doi.org/10.1029/2009GL041402
- Pruppacher, H. R., Klett, J. D., & Springer. (1997). *Microphysics of Clouds and Precipitation*. Springer. https://books.google.com/books?id=Nk40jwEACAAJ
- Reid, J. P., Bertram, A. K., Topping, D. O., Laskin, A., Martin, S. T., Petters, M. D., Pope, F. D., & Rovelli, G. (2018). The viscosity of atmospherically relevant organic particles. *Nature Communications*, 9(1), 956. https://doi.org/10.1038/s41467-018-03027-z
- Renbaum-Wolff, L., Grayson, J. W., Bateman, A. P., Kuwata, M., Sellier, M., Murray, B. J., Shilling, J. E., Martin, S. T., & Bertram, A. K. (2013). Viscosity of α-pinene secondary organic material and implications for particle growth and reactivity. *Proceedings of the National Academy of Sciences*, 110(20), 8014–8019. https://doi.org/doi:10.1073/pnas.1219548110
- Riemer, N., Ault, A. P., West, M., Craig, R. L., & Curtis, J. H. (2019). Aerosol Mixing State: Measurements, Modeling, and Impacts. *Reviews of Geophysics*, 57(2), 187–249. https://doi.org/https://doi.org/10.1029/2018RG000615
- Riipinen, I., Pierce, J. R., Yli-Juuti, T., Nieminen, T., Häkkinen, S., Ehn, M., Junninen, H., Lehtipalo, K., Petäjä, T., Slowik, J., Chang, R., Shantz, N. C., Abbatt, J., Leaitch, W. R., Kerminen, V. M., Worsnop, D. R., Pandis, S. N., Donahue, N. M., & Kulmala, M. (2011). Organic condensation: a vital link connecting aerosol formation to cloud condensation nuclei (CCN) concentrations. Atmos. Chem. Phys., 11(8), 3865–3878. https://doi.org/10.5194/acp-11-3865-2011
- Riva, M., Chen, Y., Zhang, Y., Lei, Z., Olson, N. E., Boyer, H. C., Narayan, S., Yee, L. D., Green, H. S.,
   Cui, T., Zhang, Z., Baumann, K., Fort, M., Edgerton, E., Budisulistiorini, S. H., Rose, C. A.,
   Ribeiro, I. O., e Oliveira, R. L., dos Santos, E. O., . . . Surratt, J. D. (2019). Increasing Isoprene
   Epoxydiol-to-Inorganic Sulfate Aerosol Ratio Results in Extensive Conversion of Inorganic
   Sulfate to Organosulfur Forms: Implications for Aerosol Physicochemical Properties.

- 1018 Environmental Science & Technology, 53(15), 8682–8694. 1019 https://doi.org/10.1021/acs.est.9b01019
- 1020 Roberts, G. C., & Nenes, A. (2005). A Continuous-Flow Streamwise Thermal-Gradient CCN Chamber 1021 for Atmospheric Measurements. *Aerosol Science and Technology*, 39(3), 206–221. 1022 https://doi.org/10.1080/027868290913988

- Rose, D., Gunthe, S. S., Mikhailov, E., Frank, G. P., Dusek, U., Andreae, M. O., & Pöschl, U. (2008). Calibration and measurement uncertainties of a continuous-flow cloud condensation nuclei counter (DMT-CCNC): CCN activation of ammonium sulfate and sodium chloride aerosol particles in theory and experiment. *Atmos. Chem. Phys.*, 8(5), 1153–1179. https://doi.org/10.5194/acp-8-1153-2008
- Ross, S. (1945). The Change of Surface Tension with Time. I. Theories of Diffusion to the Surface.

  Journal of the American Chemical Society, 67(6), 990–994.

  https://doi.org/10.1021/ja01222a031
- Ruehl, C. R., Chuang, P. Y., Nenes, A., Cappa, C. D., Kolesar, K. R., & Goldstein, A. H. (2012). Strong evidence of surface tension reduction in microscopic aqueous droplets. *Geophysical Research Letters*, 39(23). https://doi.org/https://doi.org/10.1029/2012GL053706
- Ruehl, C. R., Davies, J. F., & Wilson, K. R. (2016). An interfacial mechanism for cloud droplet formation on organic aerosols. *Science*, *351*(6280), 1447–1450. https://doi.org/doi:10.1126/science.aad4889
- Saukko, E., Lambe, A. T., Massoli, P., Koop, T., Wright, J. P., Croasdale, D. R., Pedernera, D. A., Onasch, T. B., Laaksonen, A., Davidovits, P., Worsnop, D. R., & Virtanen, A. (2012). Humidity-dependent phase state of SOA particles from biogenic and anthropogenic precursors. Atmos. Chem. Phys., 12(16), 7517–7529. https://doi.org/10.5194/acp-12-7517-2012
- Saxena, P., et al. (1995). Organics alter hygroscopic behavior of atmospheric particles. *Journal of Geophysical Research*: Atmospheres, 100(D9), 18755–18770. https://doi.org/https://doi.org/10.1029/95JD01835
- Schmedding, R., & Zuend, A. (2025). The role of interfacial tension in the size-dependent phase separation of atmospheric aerosol particles. *Atmos. Chem. Phys.*, *25*(1), 327–346. https://doi.org/10.5194/acp-25-327-2025
- Seinfeld, J., & Pandis, S. (1998). Atmospheric Chemistry and Physics: From Air Pollution to Climate Change.
- Seinfeld, J. H. (2003). TROPOSPHERIC CHEMISTRY AND COMPOSITION | Aerosols/Particles. In J. R. Holton (Ed.), *Encyclopedia of Atmospheric Sciences* (pp. 2349–2354). Academic Press. https://doi.org/https://doi.org/10.1016/B0-12-227090-8/00438-3
- Sheldon, C. S., Choczynski, J. M., Morton, K., Palacios Diaz, T., Davis, R. D., & Davies, J. F. (2023). Exploring the hygroscopicity, water diffusivity, and viscosity of organic–inorganic aerosols a case study on internally-mixed citric acid and ammonium sulfate particles [10.1039/D2EA00116K]. *Environmental Science: Atmospheres*, 3(1), 24–34. https://doi.org/10.1039/D2EA00116K
- Shiraiwa, M., Li, Y., Tsimpidi, A. P., Karydis, V. A., Berkemeier, T., Pandis, S. N., Lelieveld, J., Koop, T., & Pöschl, U. (2017). Global distribution of particle phase state in atmospheric secondary organic aerosols. *Nature Communications*, 8(1), 15002. https://doi.org/10.1038/ncomms15002
- Shiraiwa, M., & Seinfeld, J. H. (2012). Equilibration timescale of atmospheric secondary organic
   aerosol partitioning. Geophysical Research Letters, 39(24).
   https://doi.org/https://doi.org/10.1029/2012GL054008
- 1064 Sindelarova, K., Granier, C., Bouarar, I., Guenther, A., Tilmes, S., Stavrakou, T., Müller, J. F., Kuhn, 1065 U., Stefani, P., & Knorr, W. (2014). Global data set of biogenic VOC emissions calculated by

- the MEGAN model over the last 30 years. *Atmos. Chem. Phys.*, *14*(17), 9317–9341. https://doi.org/10.5194/acp-14-9317-2014
- Song, M., Marcolli, C., Krieger, U. K., Lienhard, D. M., & Peter, T. (2013). Morphologies of mixed organic/inorganic/aqueous aerosol droplets [10.1039/C3FD00049D]. Faraday Discussions, 165(0), 289–316. https://doi.org/10.1039/C3FD00049D
  - Spelt, J. (1996). Applied Surface Thermodynamics. Crc Press.

- Srivastava, D., Vu, T. V., Tong, S., Shi, Z., & Harrison, R. M. (2022). Formation of secondary organic
   aerosols from anthropogenic precursors in laboratory studies. npj Climate and Atmospheric
   Science, 5(1), 22. <a href="https://doi.org/10.1038/s41612-022-00238-6">https://doi.org/10.1038/s41612-022-00238-6</a>
  - Sullivan, R. C., Moore, M. J. K., Petters, M. D., Kreidenweis, S. M., Roberts, G. C., & Prather, K. A. (2009). Effect of chemical mixing state on the hygroscopicity and cloud nucleation properties of calcium mineral dust particles. *Atmos. Chem. Phys.*, 9(10), 3303–3316. https://doi.org/10.5194/acp-9-3303-2009
  - Tandon, A., Rothfuss, N. E., & Petters, M. D. (2019). The effect of hydrophobic glassy organic material on the cloud condensation nuclei activity of particles with different morphologies. *Atmos. Chem. Phys.*, 19(5), 3325–3339. https://doi.org/10.5194/acp-19-3325-2019
  - Toivola, M., Prisle, N. L., Elm, J., Waxman, E. M., Volkamer, R., & Kurtén, T. (2017). Can COSMOTherm Predict a Salting in Effect? *The Journal of Physical Chemistry A*, 121(33), 6288–6295. https://doi.org/10.1021/acs.jpca.7b04847
  - Topping, D. (2010). An analytical solution to calculate bulk mole fractions for any number of components in aerosol droplets after considering partitioning to a surface layer. *Geosci. Model Dev.*, 3(2), 635–642. https://doi.org/10.5194/gmd-3-635-2010
  - Topping, D. O., McFiggans, G. B., Kiss, G., Varga, Z., Facchini, M. C., Decesari, S., & Mircea, M. (2007). Surface tensions of multi-component mixed inorganic/organic aqueous systems of atmospheric significance: measurements, model predictions and importance for cloud activation predictions. Atmos. Chem. Phys., 7(9), 2371–2398. https://doi.org/10.5194/acp-7-2371-2007
  - Twomey, S. (1959). The nuclei of natural cloud formation part II: The supersaturation in natural clouds and the variation of cloud droplet concentration. *Geofisica pura e applicata*, *43*(1), 243–249. https://doi.org/10.1007/BF01993560
  - Twomey, S. (1974). Pollution and the planetary albedo. *Atmospheric Environment (1967)*, 8(12), 1251–1256. https://doi.org/https://doi.org/10.1016/0004-6981(74)90004-3
  - Veghte, D. P., Altaf, M. B., & Freedman, M. A. (2013). Size Dependence of the Structure of Organic Aerosol. *Journal of the American Chemical Society*, 135(43), 16046–16049. https://doi.org/10.1021/ja408903g
  - Vepsäläinen, S., Calderón, S. M., & Prisle, N. L. (2023). Comparison of six approaches to predicting droplet activation of surface active aerosol Part 2: Strong surfactants. *Atmos. Chem. Phys.*, 23(23), 15149–15164. <a href="https://doi.org/10.5194/acp-23-15149-2023">https://doi.org/10.5194/acp-23-15149-2023</a>
  - Vignes, A. (1966). Diffusion in Binary Solutions. Variation of Diffusion Coefficient with Composition.

    Industrial & Engineering Chemistry Fundamentals, 5(2), 189–199.

    https://doi.org/10.1021/i160018a007
- Virtanen, A., Joutsensaari, J., Koop, T., Kannosto, J., Yli-Pirilä, P., Leskinen, J., Mäkelä, J. M.,
  Holopainen, J. K., Pöschl, U., Kulmala, M., Worsnop, D. R., & Laaksonen, A. (2010). An
  amorphous solid state of biogenic secondary organic aerosol particles. *Nature*, 467(7317),
  824–827. <a href="https://doi.org/10.1038/nature09455">https://doi.org/10.1038/nature09455</a>
- Vitagliano, V., & Lyons, P. A. (1956). Diffusion Coefficients for Aqueous Solutions of Sodium Chloride
   and Barium Chloride. *Journal of the American Chemical Society*, 78(8), 1549–1552.
   <a href="https://doi.org/10.1021/ja01589a011">https://doi.org/10.1021/ja01589a011</a>

- Vizenor, A. E., & Asa-Awuku, A. A. (2018). Gas-phase kinetics modifies the CCN activity of a biogenic
   SOA [10.1039/C8CP00075A]. Physical Chemistry Chemical Physics, 20(9), 6591–6597.
   https://doi.org/10.1039/C8CP00075A
- 1117 Wallace, B. J., Price, C. L., Davies, J. F., & Preston, T. C. (2021). Multicomponent diffusion in 1118 atmospheric aerosol particles [10.1039/D0EA00008F]. Environmental Science: 1119 Atmospheres, 1(1), 45–55. https://doi.org/10.1039/D0EA00008F
- Wang, M., Wu, P., Sengupta, S. S., Chadhary, B. I., Cogen, J. M., & Li, B. (2011). Investigation of Water
   Diffusion in Low-Density Polyethylene by Attenuated Total Reflectance Fourier Transform
   Infrared Spectroscopy and Two-Dimensional Correlation Analysis. *Industrial & Engineering* Chemistry Research, 50(10), 6447–6454. <a href="https://doi.org/10.1021/ie102221a">https://doi.org/10.1021/ie102221a</a>

1126

1127

1131 1132

1133

1134

1135

1136

1137 1138

1139

1140

1141

1142

1143

1144

1145

1146

1147

1148

- Werner, E. K., Hammond, M., & Bain, A. (2025). Surface tension predictions during hygroscopic growth and cloud droplet activation using a simple kinetic surfactant partitioning model.

  Aerosol Science and Technology, 59(7), 781–793. https://doi.org/10.1080/02786826.2025.2465705
- Wex, H., Stratmann, F., Topping, D., & McFiggans, G. (2008). The Kelvin versus the Raoult Term in the
   Köhler Equation. Journal of the Atmospheric Sciences, 65(12), 4004–4016.
   https://doi.org/https://doi.org/10.1175/2008JAS2720.1
  - Wiedensohler, A. (1988). An approximation of the bipolar charge distribution for particles in the submicron size range. *Journal of Aerosol Science*, *19*, 387–389.
  - Wolf, M. J., Zhang, Y., Zhou, J., Surratt, J. D., Turpin, B. J., & Cziczo, D. J. (2021). Enhanced Ice Nucleation of Simulated Sea Salt Particles with the Addition of Anthropogenic Per- and Polyfluoroalkyl Substances. ACS Earth and Space Chemistry, 5(8), 2074–2085. https://doi.org/10.1021/acsearthspacechem.1c00138
  - Wu, L., Li, X., Kim, H., Geng, H., Godoi, R. H. M., Barbosa, C. G. G., Godoi, A. F. L., Yamamoto, C. I., de Souza, R. A. F., Pöhlker, C., Andreae, M. O., & Ro, C. U. (2019). Single-particle characterization of aerosols collected at a remote site in the Amazonian rainforest and an urban site in Manaus, Brazil. Atmos. Chem. Phys., 19(2), 1221–1240. https://doi.org/10.5194/acp-19-1221-2019
  - Yang, F., Chen, H., Wang, X., Yang, X., Du, J., & Chen, J. (2009). Single particle mass spectrometry of oxalic acid in ambient aerosols in Shanghai: Mixing state and formation mechanism. Atmospheric Environment, 43(25), 3876–3882. https://doi.org/https://doi.org/10.1016/j.atmosenv.2009.05.002
  - Zhang, C., Lu, M., Ma, N., Yang, Y., Wang, Y., Größ, J., Fan, Z., Wang, M., & Wiedensohler, A. (2023). Hygroscopicity of aerosol particles composed of surfactant SDS and its internal mixture with ammonium sulfate at relative humidities up to 99.9%. *Atmospheric Environment*, 298, 119625. https://doi.org/https://doi.org/10.1016/j.atmosenv.2023.119625
- Zhang, Q., Jimenez, J. L., Canagaratna, M. R., Allan, J. D., Coe, H., Ulbrich, I., Alfarra, M. R., Takami,
   A., Middlebrook, A. M., Sun, Y. L., Dzepina, K., Dunlea, E., Docherty, K., DeCarlo, P. F.,
   Salcedo, D., Onasch, T., Jayne, J. T., Miyoshi, T., Shimono, A., . . . Worsnop, D. R. (2007).
   Ubiquity and dominance of oxygenated species in organic aerosols in anthropogenically-influenced Northern Hemisphere midlatitudes. *Geophysical Research Letters*, 34(13).
   https://doi.org/https://doi.org/10.1029/2007GL029979
- Zhang, Y., Chen, Y., Lambe, A. T., Olson, N. E., Lei, Z., Craig, R. L., Zhang, Z., Gold, A., Onasch, T. B.,
   Jayne, J. T., Worsnop, D. R., Gaston, C. J., Thornton, J. A., Vizuete, W., Ault, A. P., & Surratt, J.
   D. (2018). Effect of the Aerosol-Phase State on Secondary Organic Aerosol Formation from
   the Reactive Uptake of Isoprene-Derived Epoxydiols (IEPOX). Environmental Science &
   Technology Letters, 5(3), 167–174. https://doi.org/10.1021/acs.estlett.8b00044

- Zhang, Y., Chen, Y., Lei, Z., Olson, N. E., Riva, M., Koss, A. R., Zhang, Z., Gold, A., Jayne, J. T.,
   Worsnop, D. R., Onasch, T. B., Kroll, J. H., Turpin, B. J., Ault, A. P., & Surratt, J. D. (2019a).
   Joint Impacts of Acidity and Viscosity on the Formation of Secondary Organic Aerosol from
   Isoprene Epoxydiols (IEPOX) in Phase Separated Particles. ACS Earth and Space Chemistry,
   3(12), 2646–2658. https://doi.org/10.1021/acsearthspacechem.9b00209
- 1166 Zhang, Y., Nichman, L., Spencer, P., Jung, J. I., Lee, A., Heffernan, B. K., Gold, A., Zhang, Z., Chen, Y., 1167 Canagaratna, M. R., Jayne, J. T., Worsnop, D. R., Onasch, T. B., Surratt, J. D., Chandler, D., 1168 Davidovits, P., & Kolb, C. E. (2019b). The Cooling Rate- and Volatility-Dependent Glass-Forming Properties of Organic Aerosols Measured by Broadband Dielectric Spectroscopy. 1169 1170 Environmental Science Technology, 53(21), 12366-12378. 1171 https://doi.org/10.1021/acs.est.9b03317

11731174

1175

- Zhang, Y., Sanchez, M. S., Douet, C., Wang, Y., Bateman, A. P., Gong, Z., Kuwata, M., Renbaum-Wolff, L., Sato, B. B., Liu, P. F., Bertram, A. K., Geiger, F. M., & Martin, S. T. (2015). Changing shapes and implied viscosities of suspended submicron particles. *Atmos. Chem. Phys.*, 15(14), 7819–7829. https://doi.org/10.5194/acp-15-7819-2015
- Zhu, J., Penner, J. E., Lin, G., Zhou, C., Xu, L., & Zhuang, B. (2017). Mechanism of SOA formation determines magnitude of radiative effects. *Proceedings of the National Academy of Sciences*, 114(48), 12685–12690. https://doi.org/doi:10.1073/pnas.1712273114

## **Supplemental Information:**

### Hygroscopicity of Isoprene-Derived Secondary Organic Aerosol Mixture Proxies: Importance of Diffusion and Salting In Effects

Nahin Ferdousi-Rokib<sup>1\*</sup>, N. Cazimir Armstrong<sup>2</sup>, Stephanie Jacoby<sup>3</sup>, Alana <del>J.</del> Dodero<sup>4</sup>, Martin Ahn<sup>1</sup>, Ergine R. Remy<sup>1</sup>, Zhenfa Zhang<sup>2</sup>, Avram Gold<sup>2</sup>, Joseph L. Woo<sup>5</sup>, Yue Zhang<sup>4</sup>, Jason D. Surratt<sup>2,6</sup>, Akua A. Asa-Awuku<sup>1,3</sup>

<sup>1</sup>Department of Chemical and Biomolecular Engineering, University of Maryland, College Park, MD 20742. United States

<sup>2</sup>Department of Environmental Sciences and Engineering, University of North Carolina at Chapel Hill, Chapel Hill, North Carolina 27599, United States

<sup>3</sup>Department of Chemistry and Biochemistry, University of Maryland, College Park, MD 20742, United States

<sup>4</sup>Department of Atmospheric Sciences, Texas A&M University, College Station, Texas 77843, United States

<sup>5</sup>Department of Chemical and Biomolecular Engineering, Lafayette College, Easton, PA 18042, United States

<sup>6</sup>Department of Chemistry, University of North Carolina at Chapel Hill, Chapel Hill, North Carolina 27599, United States

\*Now at: Department of Environmental Health and Engineering, Whiting School of Engineering, Johns Hopkins University, Baltimore, MD 21218, United States

#### Contents:

**LS1.** Surface Tension Solution Concentrations

H.S2. Experimental Solutions for Aerosol Measurements

**III.**S3. H-TDMA Set Up and Calibration

IV.S4. CCNC Set Up and Calibration

¥.S5. Abbreviations

VI.S6. Surface Tension Results

VII.S7. Diffusion Coefficients

VIII.S8. Impurity Information

**IX.**S9. Subsaturated Hygroscopicity Results

X.S10. Supersaturated Hygroscopicity Results

XI.S11. Goodness of Fit

XII. S12. Additional AFM Figures

 $\times 11.513.$  2-MT  $D_{\rm d}$  vs.  $\kappa_{\rm CCN}$ 

Formatted: Bullets and Numbering

# **<u>4S1</u>**. Surface Tension Solution Concentrations

Table S1. Stock solution concentrations for dilutions.

Compound	Mass (mg)	Water (mL)	Molarity (M)
2-MT	87.1	2	0.319
2-MTS	134.7	2	0.313

**Table S2.** Dilutions of 2-MT solutions for surface tension measurements.

Target 2-MT Concentration (M)	Volume of 0.3 M 2-MT Stock (µL)	Volume of UPF Water (μL)
0.003	20.0	1980.0
0.005	33.3	1966.7
0.009	60.0	1940.0
0.016	106.7	1893.3
0.030	200.0	1800.0
0.094	626.7	1373.3

**Table S3.** Dilutions of 2-MTS solutions for surface tension measurements.

Target 2-MTS Concentration (M)	Volume of 0.3 M 2-MT Stock (μL)	Volume of UPF Water (μL)
0.003	20.0	1980.0
0.009	60.0	1940.0
0.03	200.0	1800.0
0.053	353.3	1646.7
0.094	626.7	1373.3

**Table S4.** Concentrations of 2-MT/AS mixture dilutions for surface tension measurements.

Target 2-MT Concentration (mM)	Target AS Concentration (mM)	Volume of 0.3 M 2-MTS Stock (µL)	Volume of 3.5 M AS Stock (µL)	Volume of UPF Water (µL)
0.003	0.5	20	285.7	1694.3
0.009	0.5	63.2	285.7	1651.1
0.03	0.5	200	285.7	1514.3
0.09	0.5	632	285.7	1082.3

**Table S5.** Concentrations of 2-MTS/AS mixture dilutions for surface tension measurements.

Target 2-MTS Concentration (mM)	Target AS Concentration (mM)	Volume of 0.3 M 2-MTS Stock (µL)	Volume of 3.5 M AS Stock (µL)	Volume of UPF Water (µL)
0.003	0.5	20	285.7	1694.3
0.009	0.5	63.2	285.7	1651.1
0.03	0.5	200	285.7	1514.3
0.05	0.5	355.7	285.7	1358.6

## **HS2**. Experimental Solutions for Aerosol Measurements

Table S6. Solution compositions.

Mass wt% Organic (2-MT or 2-MTS sample)	Mass of Organic Sample (mg)	Mass of AS (mg)
100	10	0
90	9	1
75	7.5	2.5
60	6	4
50	5	5
40	4	6
25	2.5	7.5
10	0	10

## **IIIS3.** H-TDMA Set Up and Calibration

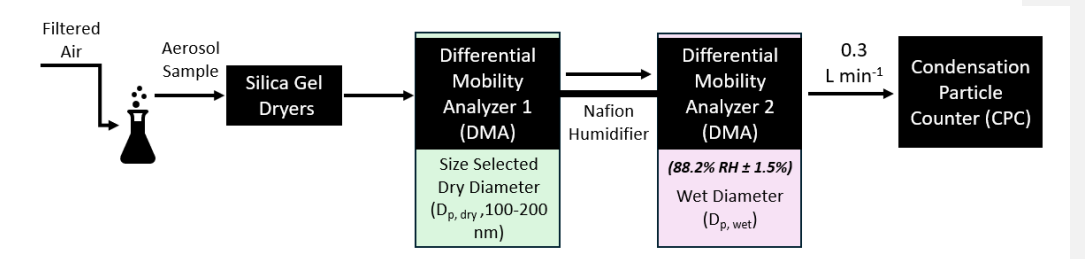


**Figure S1.** Experimental set up for H-TDMA measurements; dry, polydisperse aerosols were size selected through DMA1 at a 10:1 aerosol to sheath flow rate. The size selected particles are passed through a Nafion tube and humidified to  $89.4\% \pm 2\%$  RH. Droplet growth factor was measured using DMA2 and CPC.

Table S7. H-TDMA Ammonium Sulfate Calibration.

Size Selected Dry Diameter (nm)	Measured G <sub>F</sub>	Relative Humidity	
100	1.70	0.86	
100	1.70	0.87	
100	1.71	0.87	
100	1.71	0.87	
100	1.71	0.87	
100	1.85	0.90	
100	1.85	0.90	
100	1.72	0.87	
100	1.71	0.87	
100	1.71	0.87	
150	1.75	0.88	
150	1.75	0.88	
150	1.77	0.88	

150	1.76	0.88
150	1.89	0.90
150	1.89	0.90
150	1.76	0.88
150	1.76	0.88
150	1.77	0.88
150	1.93	0.91
150	1.93	0.91

#### **IVS4.** CCNC Set Up and Calibration

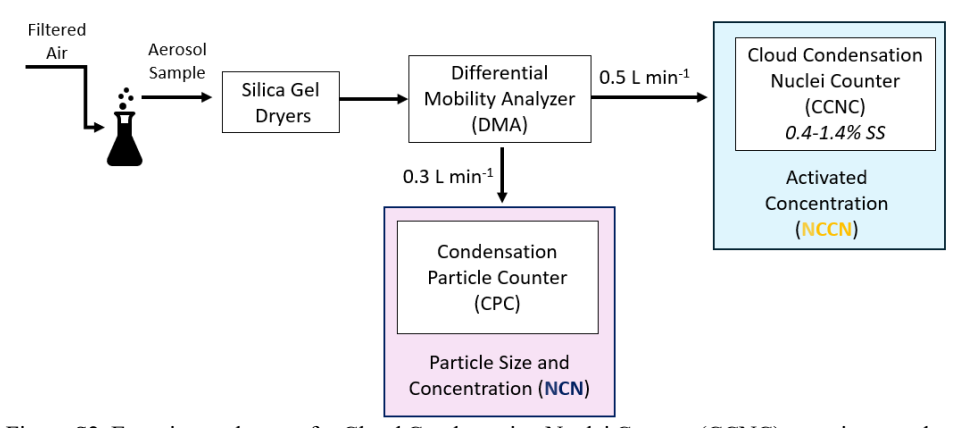


Figure S2. Experimental set up for Cloud Condensation Nuclei Counter (CCNC) experiments; dry, polydisperse aerosols were passed through the DMA at a 10:1 aerosol to sheath flow rate; aerosols were flowed into the CPC and CCN in parallel at 0.3 L min<sup>-1</sup> and 0.5 L min<sup>-1</sup>, respectively. The CPC was used to obtain NCN and the CCNC was used to obtain NCCN.

Table S8. CCNC Ammonium Sulfate Calibration.

Activation diameter (nm)	Calibrated supersaturation (%)
58.697	0.338
57.013	0.353
58.697	0.338
58.697	0.338
60.382	0.324

58.697	0.338
56.451	0.358
57.574	0.343
57.574	0.343
58.136	0.338
57.574	0.343
57.574	0.343
58.136	0.338
47.466	0.465
49.151	0.441
51.397	0.412
49.713	0.433
49.713	0.433
49.713	0.433
50.274	0.421
37.359	0.666
40.166	0.597
40.166	0.597
38.482	0.637
38.482	0.637
38.482	0.637
32.866	0.808
32.866	0.808
32.866	0.808
32.866	0.808
26.689	1.105
27.812	1.039
27.812	1.039
27.812	1.039
27.812	1.039
21.636	1.518
23.882	1.307
25.005	1.22
24.443	1.262
25.005	1.22
25.005	1.22
21.636	1.518
22.759	1.406
21.636	1.518
22.197	1.46
22.197	1.46
21.636	1.518
21.636	1.518

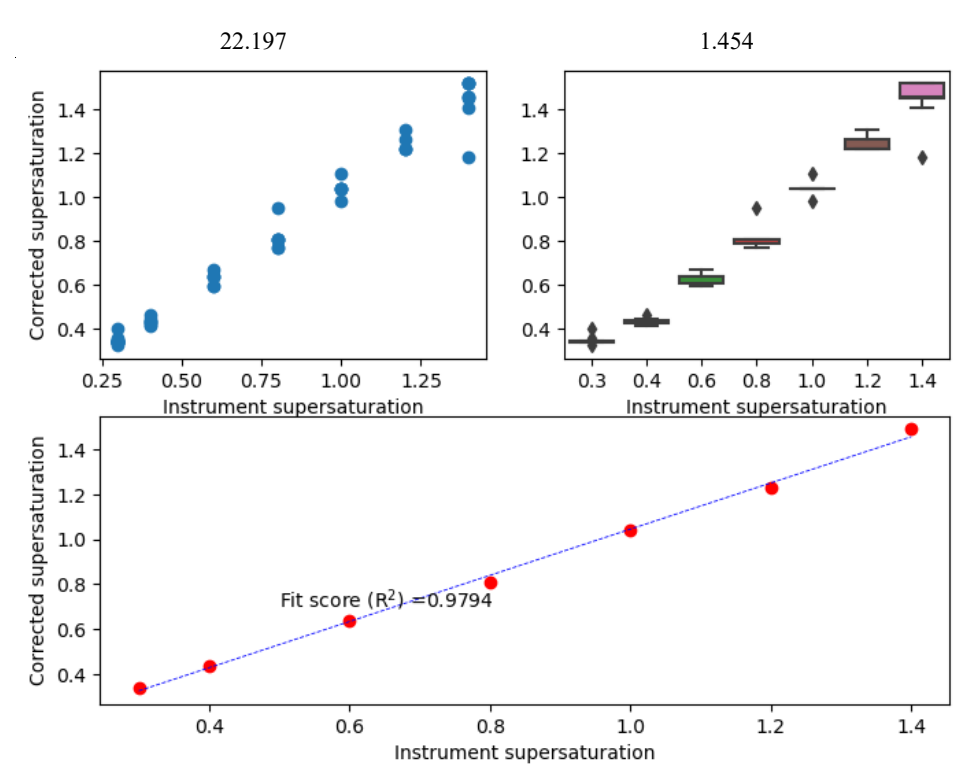


Figure S3. Ammonium sulfate (AS) CCNC instrument calibration.

## **VS5.** Abbreviations

**Table S9.** Variable abbreviations and definitions.

Abbreviation	<b>Definition</b> Organic diffusion coefficient within solvent (water) (m <sup>2</sup> s <sup>-1</sup> )	
$D_{\mathrm{s}}$		
$D_{ m w}$	Droplet wet diameter (m)	
$D_{ m d}$	Aerosol dry diameter (m)	
$D_{ m p,50}$	Critical dry diameter size where ~50% of particles activate	
SS	Supersaturation (%)	
$\kappa_{ m int}$	Intrinsic hygroscopicity based on solute physicochemical properties	
$\kappa_{ m ZSR}$	Mixture hygroscopicity based on ZSR mixing rule	
$\kappa_{ ext{H-TDMA}}$	Subsaturated hygroscopicity based on H-TDMA measurements	
KCCN	Supersaturated hygroscopicity based on CCNC measurements	

# **VIS6**. Surface Tension Results

**Table S10.** Average Surface Tension Results for 2-MT, 2-MTS, and mixtures with 500 mM AS.

Average Surface Tension (mN m<sup>-1</sup>)

	The age surface tension (m) m			
Sample Concentration (mM)	2-MT	2-MT/AS w/ 500 mM AS	2-MTS	2-MTS/AS w/ 500 mM AS
3	$72.048 \pm 0.130$	$75.296 \pm 0.108$	$73.027 \pm 0.035$	$75.131 \pm 0.246$
5	$71.753 \pm 0.029$			
9	$73.512 \pm 1.242$	$74.942 \pm 0.360$	$72.184 \pm 0.012$	$72.912 \pm 0.177$
16	$72.321 \pm 0.036$			
30	$70.713 \pm 0.479$	$74.314 \pm 0.430$	$71.426 \pm 0.067$	$72.514 \pm 0.144$
53			$69.835 \pm 0.124$	$74.177 \pm 0.173$
94	$71.279 \pm 0.004$	$72.109 \pm 0.067$	$67.950 \pm 0.241$	

 Table S11. Sodium Ethyl Sulfate Surface Tension Measurements from Peng et al., 2016.

Solute Concentration (M)	Average Surface Tension (mN m <sup>-1</sup> )	Std Dev
0.001	76.329	0.199
0.002	75.805	0.372
0.003	75.212	0.188
0.007	74.789	0.119
0.010	74.460	0.131
0.014	74.090	0.089
0.017	73.668	0.203
0.020	72.970	0.198
0.024	73.248	0.446
0.030	73.729	0.264

 Table S12.
 Sodium Methyl Sulfate Surface Tension Measurements from Peng et al., 2016.

Solute Concentration (M)	Average Surface Tension (mN m <sup>-1</sup> )	Std Dev
0.001	75.212	0.341
0.002	74.967	0.412
0.004	74.768	0.508
0.007	74.142	0.368
0.011	73.004	0.347
0.015	72.540	0.782
0.019	71.618	0.433
0.022	73.896	0.374
0.026	72.411	0.446
0.030	72.744	0.533
0.034	73.354	0.577

**Table S13.** 2-methylglutaric Acid Surface Tension Measurements from Ferdousi-Rokib et al., 2025 (in review).

Solute Concentration (M)	Average Surface Tension (mN m <sup>-1</sup> )	Std Dev
0.003	68.056	0.435
0.003	68.446	0.112
0.007	68.699	0.491
0.009	67.621	0.628
0.014	67.899	0.835

 Table S14. Sodium Octyl Sulfate Surface Tension Measurements from Peng et al., 2016.

Solute Concentration (M)	Average Surface Tension (mN m <sup>-1</sup> )	Std Dev
0.000	74.210	1.197
0.001	73.161	0.964
0.002	72.159	0.789
0.004	70.761	0.674
0.006	70.947	0.334
0.009	71.238	0.349
0.011	69.119	0.312
0.013	67.416	0.062
0.015	66.515	0.155
0.019	65.908	0.374
0.022	64.825	0.166
0.024	63.173	0.106
0.026	62.085	0.114

 Table S15.
 Sodium Doedcyl Sulfate Surface Tension Measurements.

Solute Concentration (M)	Average Surface Tension (mN m <sup>-1</sup> )	Std Dev
0.001	70.983	0.395
0.001	65.885	0.832
0.002	65.945	0.359
0.003	63.815	0.240
0.003	61.186	0.406
0.003	58.065	0.328
0.004	48.992	0.442
0.005	46.791	0.313
0.006	46.715	0.526
0.007	44.460	0.523
0.009	39.464	0.385
0.010	38.905	0.097
0.010	39.942	0.075
0.014	39.919	0.064
0.017	39.347	0.047
0.021	39.157	0.049
0.024	38.816	0.049
0.028	39.190	0.030
0.031	39.165	0.052
0.035	38.917	0.032

**Table S16.** Ammonium Sulfate Surface Tension Measurements from Ferdousi-Rokib et al., 2025 (in review).

Solute Concentration (M)	Average Surface Tension (mN m <sup>-1</sup> )	Std Dev
0.015	71.993	0.222
0.009	70.482	0.622
0.008	70.032	0.303
0.004	71.517	0.221
0.003	70.690	0.227

#### **VHS7**. Diffusion Coefficients and Viscosities

Table S17. Diffusion coefficients of 2-MT and 2-MTS in water and aqueous mixture with 500 mM AS.

Diffusion Coefficient (m² s-1)

55				
Sample Concentration (mM)	<b>2-M</b> T	2-MT/AS w/ 500 mM AS	2-MTS	2-MTS/AS w/ 500 mM AS
3	1.03E-09	8.53E-09	3.88E-09	6.57E-09
5	4.83E-09			
9	2.15E-10	7.72E-10	1.45E-10	7.7E-09
16	2.43E-10			
30	4.72E-10	1.43E-10	1.37E-10	2.75E-09
53			1.63E-10	3.88E-09
94	1.39E-11	1.091E-10	1.04E-10	

Table S18. Estimated Viscosity of 2-MT and 2-MTS at Different Conditions

	H-TDMA	Before Entering the CCNC
2-MT	0.27-0.63	8.9E4
2-MTS	22-14	3.1E8

Table S19. Estimated Diffusion Coefficient of 2-MT and 2-MTS at Different Conditions

Diffusion (cm <sup>2</sup> s <sup>-1</sup> )	H-TDMA	Before Entering the CCNC
2-MT	3.5-8.1 E-8	2.5E-13
2-MTS	1.6-4.9 E-8	1.2E-16

#### **VIIIS8**. Information on Additional Compounds

Table S20. Calibration and compound information for additional compounds

Compound	Molecular Weight (g mol <sup>-1</sup> )	Density (g cm <sup>-3</sup> )	Average surface tension (mN m <sup>-1</sup> )	к
Ammonium Sulfate ((NH <sub>4</sub> ) <sub>2</sub> SO <sub>4</sub> )	132.14 <sup>a</sup>	1.77ª	73.8	0.61
Sodium Methyl Sulfate (CH <sub>3</sub> NaO <sub>4</sub> S)	134.08 <sup>\$</sup>	1.60 <sup>\$</sup>	72.80 <sup>\$</sup>	0.459 <sup>\$</sup>

<sup>&</sup>lt;sup>a</sup>Sigma Aldrich

Table S21. Adjusted mass wt% of organic based on impurities

Mass wt% Organic (2-MTS sample)	Mass wt% of Pure 2-MTS
90	65.7
75	54.75
60	43.8
50	36.5
40	29.2
25	18.25
10	7.3

<sup>\$</sup>Peng et al 2021

# **<u>IXS9</u>**. Subsaturated Hygroscopicity Results

**Table S22.** Growth factor and subsaturated hygroscopicity results for 2-MT and 2-MT/AS mixtures.

Mass wt% 2-MT	D <sub>dry</sub> (nm)	GF	StdDev	к	StdDev
	100	1.396	0.002	0.076	0.002
100	150	1.419	0.004	0.106	0.003
	200	1.436	0.006	0.128	0.005
	100	1.518	0.001	0.353	0.001
90	150	1.534	0.002	0.369	0.002
	200	1.561	0.001	0.396	0.001
	100	1.614	0.001	0.453	0.001
75	150	1.636	0.000	0.477	0.001
	200	1.650	0.004	0.494	0.004
	100	1.717	0.002	0.482	0.002
60	150	1.702	0.002	0.466	0.002
	200	1.715	0.003	0.479	0.003
	100	1.625	0.002	0.500	0.002
50	150	1.625	0.009	0.500	0.011
	200	1.643	0.002	0.523	0.002
	100	1.689	0.002	0.586	0.003
40	150	1.705	0.001	0.606	0.002
	200	1.699	0.003	0.598	0.004
	100	1.809	0.003	0.602	0.003
25	150	1.808	0.002	0.601	0.002
	200	1.839	0.003	0.587	0.003
	100	1.877	0.000	0.608	0.004
10	150	1.872	0.027	0.627	0.007
	200	1.859	0.000	0.623	0.004

**Table S23.** Growth factor and subsaturated hygroscopicity results for 2-MTS and 2-MTS/AS mixtures.

Mass wt% 2-MTS	D <sub>dry</sub> (nm)	GF	StdDev	к	StdDev
	100	1.455	0.003	0.134	0.004
100	150	1.538	0.007	0.250	0.010
	200	1.588	0.022	0.326	0.005
	100	1.538	0.003	0.356	0.003
65.7	150	1.625	0.004	0.403	0.004
	200	1.625	0.005	0.445	0.005
	100	1.560	0.001	0.389	0.001
54.8	150	1.605	0.003	0.435	0.003
	200	1.641	0.001	0.476	0.001
	100	1.674	0.001	0.513	0.001
43.8	150	1.694	0.008	0.566	0.010
	200	1.730	0.001	0.592	0.001
	100	1.702	0.001	0.546	0.001
36.5	150	1.746	0.005	0.581	0.000
	200	1.771	0.004	0.581	0.000
	100	1.747	0.011	0.602	0.000
29.2	150	1.730	0.003	0.581	0.000
	200	1.794	0.006	0.501	0.000
	100	1.811	0.000	0.529	0.008
18.25	150	1.846	0.026	0.584	0.004
	200	1.860	0.042	0.598	0.009
	100	1.868	0.001	0.580	0.001
7.30	150	1.917	0.001	0.583	0.001
	200	1.933	0.008	0.600	0.008

## **XS10.** Supersaturated Hygroscopicity Results

**Table S24.** Supersaturated hygroscopicity results for 2-MT and 2-MT/AS mixtures.

Mass wt% 2-MT	Instrument SS	$D_{ m p,50}$	StdDev	к	StdDev
	0.318	81.300	1.337	0.102	0.020
	0.43	67.832	1.888	0.086	0.027
	0.653	50.528	0.852	0.105	0.018
100	0.876	41.218	0.722	0.105	0.019
	1.099	34.767	0.000	0.138	0.000
	1.323	29.928	0.000	0.171	0.000
	1.546	25.694	1.075	0.221	0.029
	0.324	75.859	1.294	0.300	0.016
	0.427	62.040	0.693	0.316	0.010
	0.633	46.810	2.240	0.341	0.061
90	0.839	38.638	0.866	0.343	0.023
	1.045	32.831	0.000	0.360	0.000
	1.251	27.412	0.474	0.433	0.022
	1.458	23.517	0.469	0.505	0.030
	0.324	72.509	0.930	0.344	0.014
	0.427	60.412	0.780	0.342	0.014
	0.633	45.950	1.031	0.355	0.022
75	0.839	36.702	0.000	0.398	0.000
	1.045	29.928	0.000	0.475	0.000
	1.251	27.267	0.419	0.439	0.020
	1.458	23.431	0.437	0.511	0.028
	0.324	63.155	0.994	0.520	0.023
	0.427	52.626	0.482	0.517	0.016
	0.633	40.036	0.663	0.536	0.027
60	0.839	33.799	0.866	0.512	0.039
	1.045	28.315	0.456	0.561	0.026
	1.251	25.283	0.387	0.551	0.024
	1.458	22.186	0.000	0.601	0.000
	0.324	63.509	0.619	0.517	0.020
	0.427	53.584	1.217	0.495	0.034
	0.633	41.541	0.838	0.486	0.026
50	0.839	34.961	0.387	0.470	0.015
	1.045	29.283	0.456	0.517	0.024
	1.251	26.057	0.000	0.512	0.000
	1.458	22.463	0.437	0.591	0.033
	0.324	60.808	0.964	0.581	0.031
40	0.427	51.509	0.619	0.550	0.019
τU	0.633	40.670	0.677	0.509	0.026
	0.839	33.993	0.387	0.501	0.017

	1.045	29.928	0.000	0.473	0.000
	1.251	26.057	0.000	0.502	0.000
	1.458	22.401	0.402	0.583	0.030
	0.324	60.654	0.640	0.585	0.017
	0.427	50.735	0.484	0.577	0.014
	0.633	40.397	0.556	0.521	0.023
25	0.839	34.041	0.803	0.499	0.036
	1.045	28.960	0.000	0.524	0.000
	1.251	25.250	0.361	0.553	0.023
	1.458	23.033	0.320	0.537	0.022
	0.324	59.848	1.004	0.610	0.031
	0.427	50.832	0.474	0.573	0.017
	0.633	40.159	0.479	0.530	0.018
10	0.839	32.831	0.000	0.555	0.000
	1.045	28.960	0.000	0.522	0.000
	1.251	25.283	0.387	0.550	0.024
	1.458	22.831	0.456	0.551	0.034

**Table S25.** Supersaturated hygroscopicity results for 2-MT and 2-MT/AS mixtures.

Mass wt% 2-MTS	Instrument SS	$D_{ m p,50}$	StdDev	к	StdDev
	0.318	78.688	1.289	0.164	0.020
	0.430	65.654	1.830	0.135	0.028
	0.653	49.864	1.313	0.132	0.027
100.0	0.876	42.348	0.361	0.102	0.010
	1.099	35.735	0.000	0.123	0.000
	1.323	30.702	1.129	0.143	0.032
	1.546	27.872	0.320	0.151	0.015
	0.318	73.638	0.954	0.342	0.015
	0.430	61.248	0.622	0.325	0.011
	0.653	47.670	0.456	0.299	0.008
65.7	0.876	39.606	0.000	0.292	0.000
	1.099	32.638	0.387	0.333	0.012
	1.323	29.202	0.419	0.321	0.013
	1.546	26.178	0.320	0.327	0.011
	0.318	72.286	1.084	0.364	0.016
	0.430	59.638	1.064	0.353	0.016
	0.653	47.133	0.402	0.312	0.008
54.8	0.876	38.396	0.419	0.325	0.011
	1.099	33.799	0.000	0.303	0.000
	1.323	28.960	0.000	0.333	0.000
	1.546	25.694	0.674	0.351	0.026
	0.318	67.231	0.634	0.446	0.011
	0.430	56.585	1.041	0.410	0.022
	0.653	44.251	0.843	0.372	0.021
43.8	0.876	35.735	0.000	0.395	0.000
	1.099	30.896	0.000	0.389	0.000
	1.323	27.025	0.000	0.402	0.000
	1.546	24.122	0.000	0.415	0.000
	0.318	66.461	1.318	0.459	0.029
	0.430	56.272	0.608	0.412	0.011
	0.653	44.030	0.874	0.377	0.020
36.5	0.876	35.735	0.000	0.394	0.000
	1.099	31.283	0.474	0.374	0.017
	1.323	27.025	0.000	0.401	0.000
	1.546	23.517	0.469	0.448	0.026
	0.318	63.638	1.415	0.523	0.032
	0.430	53.832	0.620	0.472	0.019
29.2	0.653	41.420	0.756	0.450	0.026
∠ <b>J</b> .∠	0.876	34.961	0.022	0.418	0.022
	1.099	29.154	0.387	0.462	0.018
	1.323	26.057	0.000	0.447	0.000

	1.546	22.428	0.419	0.515	0.027
	0.318	64.203	1.149	0.517	0.025
	0.430	52.802	0.622	0.508	0.021
	0.653	42.785	1.123	0.418	0.029
18.3	0.876	34.767	0.000	0.436	0.000
	1.099	29.686	0.803	0.447	0.035
	1.323	26.057	0.000	0.456	0.000
	1.546	22.186	0.000	0.542	0.000
	0.318	59.840	0.767	0.632	0.024
	0.430	51.219	0.433	0.553	0.013
	0.653	40.358	0.887	0.491	0.033
7.3	0.876	32.831	0.000	0.510	0.000
	1.099	29.154	0.387	0.464	0.018
	1.323	25.089	0.000	0.503	0.000
	1.546	22.186	0.000	0.534	0.000

## **XIS11**. Goodness of Fit

**Table S26.** Köhler Theory  $R^2$ .

 $\kappa_{\rm ZSR} R^2$ 

Mixture	H-TDMA	CCN
2-MT/AS	0.686	0.787
2-MTS/AS	0.913	0.972

# **XII**<u>S12</u>. Additional AFM Figures

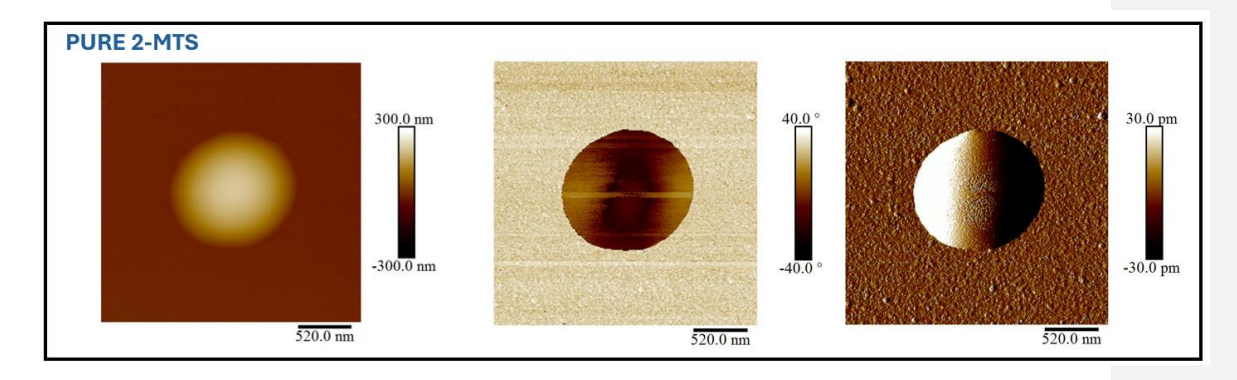


**Figure S4.** AFM Image of 100wt% synthesized 2-MTS and visualization. The figure shows the height, phase, and amplitude error from left to right.

## $\times 111513$ . 2-MT $D_{\rm d}$ vs $\kappa_{\rm CCN}$

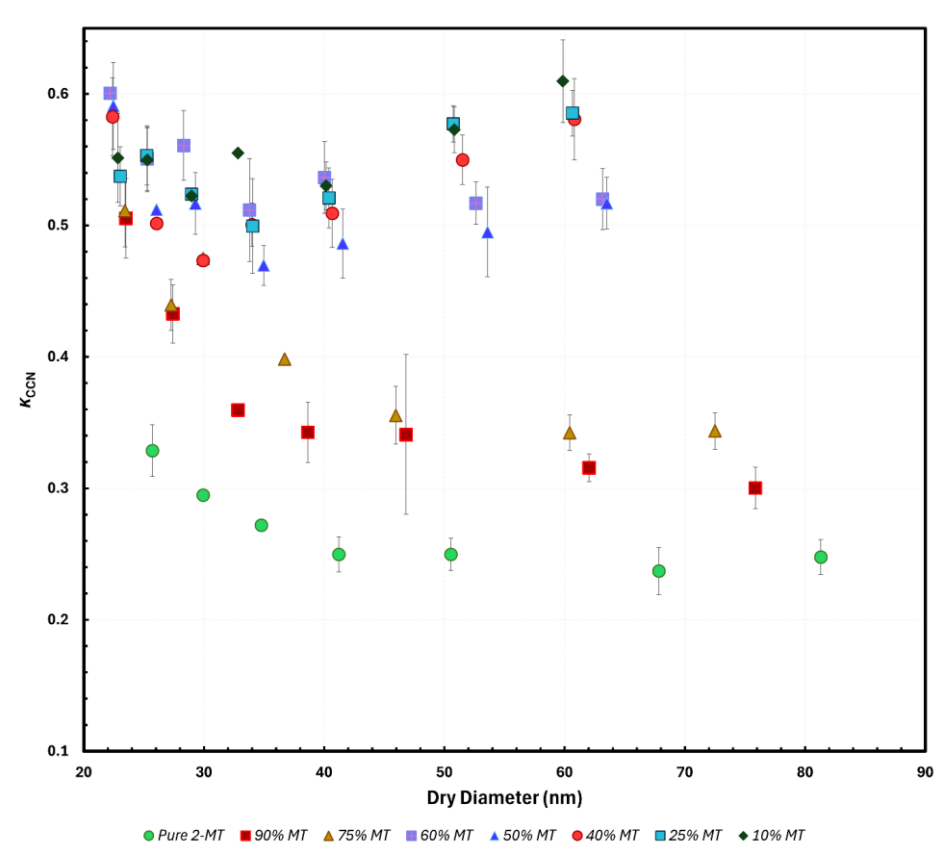


**Figure S5.** 2-MT  $D_d$  vs  $\kappa_{CCN}$  of all mixtures and 100 wt% 2-MT aerosols.